HHS Public Access

Author manuscript

*Dev Biol*. Author manuscript; available in PMC 2017 September 19.

Published in final edited form as:

*Dev Biol*. 2017 September 01; 429(1): 306–320. doi:10.1016/j.ydbio.2017.06.015.

# Novel functions for the RNA-binding protein ETR-1 in *Caenorhabditis elegans* reproduction and engulfment of germline apoptotic cell corpses

**Ruby Boateng**[a], **Ken C.Q. Nguyen**[b], **David H. Hall**[b], **Andy Golden**[c], and **Anna K. Allen**[a,*]

[a]Department of Biology, Howard University, Washington, DC 20059, USA

[b]Center for C. elegans Anatomy, Albert Einstein College of Medicine, New York, NY 10461, USA

[c]National Institutes of Diabetes and Digestive and Kidney Diseases, National Institutes of Health, Bethesda, MD 20892, USA

## Abstract

RNA-binding proteins (RBPs) are essential regulators of gene expression that act through a variety of mechanisms to ensure the proper post-transcriptional regulation of their target RNAs. RBPs in multiple species have been identified as playing crucial roles during development and as having important functions in various adult organ systems, including the heart, nervous, muscle, and reproductive systems. ETR-1, a highly conserved ELAV-Type RNA-binding protein belonging to the CELF/Bruno protein family, has been previously reported to be involved in *C. elegans* muscle development. Animals depleted of ETR-1 have been previously characterized as arresting at the two-fold stage of embryogenesis. In this study, we show that ETR-1 is expressed in the hermaphrodite somatic gonad and germ line, and that reduction of ETR-1 via RNA interference (RNAi) results in reduced hermaphrodite fecundity. Detailed characterization of this fertility defect indicates that ETR-1 is required in both the somatic tissue and the germ line to ensure wild-type reproductive levels. Additionally, the ability of ETR-1 depletion to suppress the published WEE-1.3-depletion infertility phenotype is dependent on ETR-1 being reduced in the soma. Within the germline of *etr-1(RNAi)* hermaphrodite animals, we observe a decrease in average oocyte size and an increase in the number of germline apoptotic cell corpses as evident by an increased number of CED-1::GFP and acridine orange positive apoptotic germ cells. Transmission Electron Microscopy (TEM) studies confirm the significant increase in apoptotic cells in ETR-1-depleted animals, and reveal a failure of the somatic gonadal sheath cells to properly engulf dying germ cells in *etr-1(RNAi)* animals. Through investigation of an established engulfment pathway in *C. elegans*, we demonstrate that co-depletion of CED-1 and ETR-1 suppresses both the reduced fecundity and the increase in the number of apoptotic cell corpses observed in *etr-1(RNAi)* animals. Combined, this data identifies a novel role for ETR-1 in hermaphrodite gametogenesis and in the process of engulfment of germline apoptotic cell corpses.

*Corresponding author.

**Keywords**

ETR-1; *C. elegans* reproduction; RNA-binding protein; Physiological germline apoptosis; Engulfment; CED-1

## 1. Introduction

RNA-binding proteins (RBPs) play critical roles in controlling gene expression through post-transcriptional regulation of specific target RNAs. Studies in several species have established the essential function of RNA regulation via RBPs in the germ line and throughout early embryonic development (Colegrove-Otero et al., 2005; Detwiler et al., 2001; Lee and Schedl, 2006; Richter and Lasko, 2011). During oogenesis, translational regulation is of the utmost importance, as the oocytes of most animals are transcriptionally quiescent. Therefore, mRNAs must be transcribed by the mother in the early germ line and stored in the oocytes prior to fertilization to be available for translation in the newly formed zygote (reviewed by Li et al., 2010; Robertson and Lin, 2013). In the nematode *Caenorhabditis elegans* at least 20 of the approximately 500 genes annotated to encode RBPs play an essential function in the germ line and early embryonic development (Lee and Schedl, 2006).

ETR-1 (*E*LAV-*T*ype *R*NA-binding protein) in *C. elegans* is one of two members belonging to the highly conserved CELF/Bruno RNA-binding protein family, the other being ETR-1's paralog UNC-75 (Milne and Hodgkin, 1999; WormBase: etr-1, www.wormbase.org). Most species possess multiple (3–10) members of the CELF/Bruno protein family, with individual members typically having distinct roles in the nervous system, muscle, brain, heart, and/or reproductive tissues/organs (Barreau et al., 2006; Dasgupta and Ladd, 2012). ETR-1 has been previously shown to play a developmental role in muscle formation and function, while UNC-75 plays a role in the nervous system (Loria et al., 2003; Milne and Hodgkin, 1999). The *etr-1* locus is complex resulting in 19 coding isoforms and 1 noncoding isoform (Supplementary Fig. S1) (WormBase: etr-1, www.wormbase.org). Notably, in other organisms several members of the CELF/Bruno family are subjected to high levels of alternative splicing, generating multiple protein isoforms that exhibit isoform-specific tissue expression and varying temporal expression (Barreau et al., 2006; Li et al., 2001). Each ETR-1 isoform possesses between one to three highly conserved RNA Recognition Motifs (RRMs) which are domains that are capable of binding single-stranded RNA and enabling the RBP to interact with its target mRNAs (Supplementary Fig. S1) (Cléry et al., 2008; Maris et al., 2005; WormBase: etr-1, www.wormbase.org). A COBALT alignment of all 19 ETR-1 isoforms with their paralog UNC-75 and three predicted homologues (human CUGbp1, *Drosophila* Bruno-2, and *Drosophila* ELAV), shows the highest conservation of amino acids within the RRMs (Supplementary Fig. S2) (Papadopoulos and Agarwala, 2007). Interestingly, there are currently no RNA targets identified for ETR-1, but potential neuronal targets have been recently identified for UNC-75 (Chen et al., 2016; Lee and Schedl, 2006; WormBase: etr-1, www.wormbase.org).

We previously identified ETR-1 in a screen for suppressors of the highly penetrant infertility associated with depletion of the WEE-1.3 inhibitory kinase involved in oocyte meiotic arrest and oocyte maturation (Allen et al., 2014). Others have reported that RNAi depletion of ETR-1 in sensitized strain backgrounds results in fertility defects, including a reduced brood size and sterility (Ceron et al., 2007; Rual et al., 2004). Additionally, it has been previously reported that homologues of ETR-1 in both *Drosophila* and mouse show impaired fertility, exhibiting reproductive defects during both oogenesis and spermatogenesis (Castrillon et al., 1993; Dev et al., 2007; Kress et al., 2007; Schupbach and Wieschaus, 1991). These data taken together suggest a potential reproductive role for ETR-1 within *C. elegans*.

In the *C. elegans* hermaphrodite, the reproductive organ, or gonad, is a U-shaped, bi-lobed structure that consists of both a germline and a somatic component (Greenstein, 2005; Hubbard and Greenstein, 2000). The germ line is capable of producing both sperm and oocytes, with sperm production occurring first and then the hermaphrodite switching to oocyte production (Corsi et al., 2015; Hubbard and Greenstein, 2005). Spermatogenesis begins during the animal's third larval stage, is completed by the fourth larval stage, and all the spermatids are stored in the spermatheca where the first ovulation triggers them to complete spermiogenesis (L'Hernault, 2006). Oogenesis begins in the early young adult developmental stage, with the distal most female germ cells undergoing mitosis to expand the number of germ cells, and then switching to meiosis prior to the bend of the gonad arm (Greenstein, 2005). The germ cell nuclei are initially separated by incomplete plasma membranes, and thus maintain a connection with a common cytoplasmic gonadal core through which mRNAs and proteins can pass (Wolke et al., 2007). During the late stages of oogenesis, in the proximal most region of the gonad, the oocytes complete cellularization and the individualized oocytes await meiotic maturation, ovulation into the spermatheca, and subsequent fertilization (Greenstein, 2005).

The somatic gonad is comprised of five tissues: the distal tip cells (DTCs), five pairs of gonadal sheath cells, the spermatheca, the spermatheca-uterine valves and the uterus (Lints and Hall, 2009a). The gonadal sheath cells (pairs 1–5) cover and closely associate with the germ line of each gonadal arm. Individual sheath cells can be recognized by their location along the gonad proximal-distal axis (Hall et al., 1999). Sheath cell 1 is the distal-most and wedges filopodia between the distal germ cells existing in the syncytial gonad environment (Hall et al., 1999; Lints and Hall, 2009b). Sheath cell 5 is the proximal-most, covering the developing and maturing oocytes (Lints and Hall, 2009b). The sheath cells are instrumental for promoting germline proliferation and exit from meiotic pachytene (pairs 1 and 2); physiological germline apoptosis (pair 3 and a portion of pair 2); and oocyte maturation and ovulation (pairs 4 and 5) (Greenstein, 2005; Hall et al., 1999; Lints and Hall, 2009a).

The goal of the present work is to investigate the function of ETR-1 during *C. elegans* hermaphrodite reproduction. We show that ETR-1 is necessary in both the somatic gonad and the germ line in order to enable an animal to reach full reproductive capacity. Additionally, through antibody staining, we demonstrate that ETR-1 is expressed not only in the muscle, as previously reported, but also in the germ line in both developing oocytes and mature sperm. Finally, our results implicate ETR-1 in physiological germline apoptosis, most likely playing a role in the engulfment of apoptotic germ cell corpses. This study thus

demonstrates that ETR-1 is playing a previously unappreciated role during *C. elegans* oogenesis, and may help advance our understanding of the multiple functions that this particular member of the CELF/Bruno protein family is playing.

## 2. Materials and methods

### 2.1 Nematode strains and culture conditions

The following C. elegans strains were used in this work: Bristol strain N2, NL2098 [rrf-1(pk1417) I], NL3511 [ppw-1(pk1425) I], etr-1(tm6221)/egl-26(ku228), MD701 (bcIs39[lim-7p::ced-1::GFP + lin-15(+)]), CB3203 [ced-1(e1735)], MT2405 [ced-3(n717) unc-26(e205) IV], and MT2551 [ced-4(n1162) dpy-17(e164) III]. All strains were grown and maintained under standard conditions at 20° (Brenner, 1974).

### 2.2 RNA Interference (RNAi)

RNAi experiments were performed via feeding using HT115(DE3) bacterial cells seeded on MYOB plates containing 2 mM IPTG and 25 μg/ml carbenicillin (Allen et al., 2014; Timmons and Fire, 1998). RNAi constructs were obtained from the Open Biosystems ORF-RNAi library (Huntsville, AL) and sequence verified prior to usage. The *etr-1* RNAi construct (Plate 10014C9 in the library) contains the entire *etr-1* coding region (see Supplementary Fig. S1, exons 2–13). L4 hermaphrodites were fed the RNAi constructs for 20–24 h at 24° (Day 1). Animals were then singled to individual, new RNAi plates for another 24 h at 24° (Day 2). The hermaphrodites were then removed from each plate and the plates were incubated for an additional 24 h at 20° prior to the scoring and characterization of the resultant brood. The brood size analysis was conducted by counting all animals on the plate (embryos younger than two-fold; two-fold embryos, dying embryos and larvae). Controls used were dsRNA against: (1) *smd-1(F47G4.7)*, referred to as *control(RNAi)* throughout this report, this construct triggers the RNAi response, but has no reportable phenotypic effect (Andy Golden and Kevin O'Connell, personal communication); and (2) *wee-1.3(Y53C12A.1)* which produces a sterile phenotype and confirms RNAi plates are working. For co-depletions or RNAi using two dsRNAs, bacterial cells were individually grown overnight and then mixed in equal volume before seeding.

### 2.3 Live Imaging

Animals were placed on a slide with a 3% agarose pad and a drop of 0.2 mM levamisole diluted in M9 buffer. A coverslip was placed onto the slide, sealed with nail polish and allowed to dry. Images were taken using spinning-disk confocal microscopy as described below.

### 2.4 Microscopy

Fluorescent images of live or fixed samples were captured using a Nikon Ti-E-PFS inverted spinning-disk confocal microscope equipped with a 60× 1.4 NA Plan Apo Lambda objective. The system is outfitted with a Yokogawa CSU-X1 spinning disk unit, a self-contained 4-line laser module (excitation at 405, 488, 561, and 640 nm), and Andor iXon 897 EMCCD camera. Confocal fluorescent images and DIC images were acquired and processed using the Nikon NIS-Elements and Adobe Photoshop CS5 software.

### 2.5 Ovulation rate

RNAi was performed on L4 hermaphrodites as described above followed by ovulation rates as described in (McGovern et al., 2007).

### 2.6 Germ line and oocyte size assays

L4 hermaphrodites were subject to RNAi and prepared for imaging as described in the RNAi ovulation rate and live imaging sections. Images of individual gonad arms were taken using differential interference contrast (DIC) microscopy. The lengths of the gonad arm and the uterus, and the area of individual oocytes were measured with Nikon NIS-Elements software and data analyzed using Microsoft Excel.

### 2.7 Mitotic index

The mitotic index was determined in the RNAi-treated animals utilizing the number and position of phospho-histone H3 (pH3) positive germline nuclei as previously described in Crittenden et al. (2006). The mitotic region was defined as extending from the distal tip cell to the distal edge of the transition zone (TZ), with the TZ being identified via the presence of crescent shaped nuclei.

### 2.8 Staining germline apoptotic cells using acridine orange (AO)

An acridine orange assay for germline apoptotic cells was performed as described by Lant and Derry (2014). L4 hermaphrodites were depleted of ETR-1 or a control gene for 24 h at 24°. Acridine orange (diluted in M9 buffer to a final concentration of 75 μg/ml) was added to animals on each RNAi plate. All plates were incubated at 24° for 1–2 h. Animals were then transferred to a new RNAi plates without the acridine orange and incubated for 1 h at 24°. Animals were viewed as described in the Live Imaging section.

### 2.9 Transmission electron microscopy (TEM)

ETR-1 and control-depleted animals were treated for 16–20 h as described above. For fixation for TEM, the conventional two-step fixation (Hall, 1995) was followed. Digital images were collected from thin sections on a Philips CM10 TEM using an Olympus Morada camera.

### 2.10 Generation of anti-ETR-1 antibody

A polyclonal, rabbit antibody to ETR-1 (PA5042) was generated using a custom antibody service (Pierce Biotechnology/Thermo Scientific, Rockford, IL) to a region within exon 13 that encodes the extreme C-terminal peptide sequence KRLKVQLKVDRGNPYNR.

### 2.11 Immunofluorescence

Adult hermaphrodite germ lines were stained using the immunofluorescence method described in (Allen et al., 2014). Primary antibodies utilized were: rabbit anti-ETR-1 (1:400; this study), mouse anti-myosin heavy chain A (5–6; final concentration of 2.5 μg/ml; Developmental Studies Hybridoma Bank), rabbit anti-phospho-histone H3(Ser10) (1:200; Upstate Biotechnology, Waltham, MA), and mouse anti-nuclear pore complex Mab414 (1:500, Abcam, Cambridge, MA). Secondary antibodies were: goat-anti-mouse or goat-anti-

rabbit Alexa Fluor 488-conjugated or 568-conjugated (1:1000; Invitrogen, Grand Island, NY).

## 3. Results

### 3.1 ETR-1 plays a role in both the somatic and germline tissues to influence C. elegans fertility and embryonic survival

To determine whether ETR-1 plays a role during *C. elegans* reproduction and whether that role is dependent on ETR-1 being expressed in somatic tissue, germline tissue, or both tissues of the hermaphrodite, we depleted ETR-1 via RNAi feeding in wild-type (N2) animals and RNAi deficient mutant strains. Specifically we utilized *rrf-1(pk1417)* animals that are RNAi deficient in most somatic tissues and *ppw-1(pk1425)* animals that are RNAi deficient in the germ line (Kumsta and Hansen, 2012; Tijsterman et al., 2002; Yigit et al., 2006). RNAi depletion of ETR-1 in wild-type animals results in a moderate yet significant decrease in the average 24 h brood compared to control depleted animals (Fig. 1A, compare bars #1 and #4, *control(RNAi)* = 174 brood, *etr-1(RNAi)* = 118 brood, p-value < 0.0001). A decrease in brood size upon depletion of ETR-1 is also observed in the somatic RNAi defective strain [*rrf-1(pk1417)*] and in the germline RNAi defective strain [*ppw-1(pk1425)*] (Fig. 1A, compare black bars #2 to #5 for *rrf-1* data and grey bars #3 to #6 for *ppw-1* data). In our hands, the *rrf-1(pk1417)* strain exhibits a moderately reduced brood compared to wild-type animals when fed *control(RNAi)* and grown at 24° (Fig. 1A, compare bars #1 to #2, wild-type *control(RNAi)* = 174 brood, *rrf-1(pk1417) control(RNAi)* = 139 brood, p-value < 0.0001). We have not investigated this further. As depletion of ETR-1 only in the somatic tissue and depletion only in the germline tissue both result in reduced fertility, these results suggest that ETR-1 is required in both the somatic tissue and the germ line to ensure normal fertility levels of the *C. elegans* hermaphrodite.

For all strains and RNAi conditions analyzed, there was no delay in the appearance of the brood, which might have biased the 24 h limited brood analysis (data not shown). Moreover, in ETR-1 single depleted and co-depleted animals a portion of the resultant progeny exhibits the PAT (paralyzed at the two-fold stage) phenotype previously reported, thereby validating that RNAi depletion of ETR-1 is functioning (see below and Fig. 1B) (Milne and Hodgkin, 1999). Furthermore, we designed and tested two additional ETR-1 RNAi clones that also resulted in reduced fertility and embryonic arrest at the PAT developmental stage (data not shown). Additionally, there is a 454 base pair *etr-1* deletion mutant [*etr-1(tm6221)*] available that is homozygous early embryonic lethal (C. elegans Deletion Mutant Consortium, 2012). However, heterozygous animals balanced over *egl-26(ku228)* exhibit a reduced brood and an increase in embryonically arrested progeny compared to wild-type animals (data not shown). Finally, we depleted UNC-75, the paralog of ETR-1, in wild-type animals, and observed no fertility defect (data not shown). Taken together all of this data strongly suggests that ETR-1 is the CELF/BRUNO family member required during reproduction for wild-type hermaphrodite fertility levels.

Interestingly, the terminal phenotype of the brood is altered when RNAi cannot occur in the soma (Fig. 1B). Wild-type animals subjected to *etr-1(RNAi)* give rise to broods that exhibit a 98.5% embryonic arrest, with a significant portion of those embryos (87%) arresting at the

two-fold stage (Fig. 1B, wild-type *etr-1(RNAi)*; bar #4; red portion of the bar). Our result is consistent with previously published research characterizing depletion of ETR-1 as resulting in a PAT phenotype (Milne and Hodgkin, 1999). However, when somatic RNAi defective animals [*rrf-1(pk1417)*] are subjected to *etr-1(RNAi)* there is only a 56% embryonic arrest, with 38% of the brood arresting at the two-fold embryo stage, while 44% of the brood hatches and enters the larval stage (Fig. 1B, *rrf-1(pk1417) etr-1(RNAi)*; bar #5; red and purple portion of the bar, respectively). Similarly, we observe a decrease in the degree of embryonic arrest exhibited when germline RNAi defective animals [*ppw-1(pk1425)*] are depleted of ETR-1 (Fig. 1B, *ppw-1(pk1425) etr-1(RNAi)*; bar #6; red portion of the bar). These results suggest that the two-fold arrest phenotype requires depletion of ETR-1 in both the soma and the germ line, because animals unable to perform either somatic or germline RNAi exhibit a reduced percentage of PAT embryos than wild-type animals depleted of ETR-1.

### 3.2 Suppression of the WEE-1.3 depletion infertility phenotype by co-depletion of ETR-1 is dependent on somatic RNAi

We had previously identified a potential reproductive role for ETR-1 when the gene arose in a candidate screen for suppressors of the highly penetrant *wee-1.3(RNAi)* infertility phenotype (Allen et al., 2014). Wild-type or somatic RNAi defective animals depleted of WEE-1.3 are sterile compared to animals fed a control RNAi (Fig. 1A, compare bars #1 and #10 or bars #2 and #11; wild-type *control(RNAi)* = 174 brood, wild-type *wee-1.3(RNAi)* = 0.3 brood, *rrf-1(pk1417) control(RNAi)* = 139 brood, *rrf-1(pk1417) wee-1.3(RNAi)* = 1.5 brood; p-values < 0.0001). The small brood (average of 1.5 progeny per hermaphrodite) that emerges when *wee-1.3(RNAi)* is performed in an *rrf-1(pk1417)* strain consists of mostly hatched animals (61% of the total brood are larvae) and is likely a result of incomplete knockdown of WEE-1.3 (Fig. 1B, *rrf-1(pk1417) wee-1.3(RNAi)*; bar #11; purple portion of the bar). Co-depletion of ETR-1 and WEE-1.3 in wild-type animals results in suppression of the infertility phenotype observed upon single depletion of WEE-1.3 (Fig. 1A, compare bars #10 and #16; wild-type *wee-1.3(RNAi)* = 0.3 brood, *wee-1.3/etr-1(RNAi)* = 15.4 brood; p-value < 0.0001). While this brood (average of 15.4 progeny per hermaphrodite) is smaller than the brood of a control treated animal, this represents a significant increase in fertility considering that *wee-1.3(RNAi)* animals are completely sterile (p-value < 0.0001). Additionally, 86% of this brood is arrested during embryonic development (Fig. 1B, wild-type *wee-1.3/etr-1(RNAi)*; bar #16; blue, red and green portions of the bar). Interestingly, of the 86% embryonic arrest, a majority (79%) are arrested prior to the PAT phenotype (Fig. 1B, wild-type *wee-1.3/etr-1(RNAi)*; bar #16; blue portion of the bar). Co-depletion of ETR-1's paralog, UNC-75, and WEE-1.3 does not suppress the WEE-1.3 infertility phenotype (data not shown).

In the *rrf-1(pk1417)* somatic RNAi defective line, the suppression of the WEE-1.3-depletion infertility observed upon co-depletion of WEE-1.3 and ETR-1 is abolished, and the co-depleted *rrf-1(pk1417)* mothers remain infertile (Fig. 1A, compare bars #16 and #17; wild-type *wee-1.3/etr-1(RNAi)* = 15.4 brood, *rrf-1(pk1417) wee-1.3/etr-1(RNAi)* = 0.7 brood; p-value < 0.0001). This data implies that ETR-1 levels must be reduced in the somatic tissue in order to achieve suppression of the WEE-1.3-depletion infertility phenotype. In the

*ppw-1(pk1425)* germline RNAi defective lines, *wee-1.3(RNAi)* does not result in infertility (Fig. 1A, compare bars #3 and #12; *ppw-1(pk1425) control(RNAi)* = 174.2 brood, *ppw-1(pk1425) wee-1.3(RNAi)* = 177.6 brood; p-value = 0.29). This shows that the WEE-1.3-depletion infertility is due to WEE-1.3 being reduced specifically in the germ line. As our suppression assay is dependent on the *wee-1.3(RNAi)* treated animals being sterile, we are unable to test whether co-depletion of ETR-1 and WEE-1.3 in only the soma is sufficient for ETR-1 depletion to suppression the WEE-1.3-depleted infertility (Fig. 1A, compare bars #3, #12, and #18). One alternative interpretation to the above suppression data is that when both *wee-1.3* and *etr-1* dsRNAs are present, the RNAi effect is mutually weakened. We do not believe this is the case for animals co-depleted of WEE-1.3 and ETR-1 because when we conduct qRT-PCR on germ lines dissected from co-depleted animals we can show that the levels of *wee-1.3* are decreased (data not shown), and a percentage of the brood resulting from the co-depleted animals has the reported PAT phenotype indicative that ETR-1 levels have been reduced (Fig. 1B).

### 3.3 ETR-1 is localized in both the somatic and germline portions of the hermaphrodite gonad

ETR-1 expression was previously shown to be muscle specific (Milne and Hodgkin, 1999). This data was determined by analyzing a transgenic animal containing a transcriptional fusion reporter where 4 kb of upstream sequence and the first exon of *etr-1* was fused to a GFP-β-galactosidase reporter (Milne and Hodgkin, 1999). Notably, no expression was reported in the gonad, which is not surprising as we now know that multicopy transgenes, such as those generated via microinjection and which were standard at the time, are often silenced in the germ line (Kelly et al., 1997; Merritt and Seydoux, 2010). Due to the fertility data presented above implicating a role for ETR-1 in reproduction, we wanted to determine whether ETR-1 exhibits expression in the hermaphrodite gonad. Therefore, we generated an ETR-1 polyclonal antibody (PA5042) that recognizes a common C-terminal region found in exon 13 that is present in all 19 of the predicted coding ETR-1 isoforms (see Supplementary Fig. S1). We found that ETR-1 is expressed in both the germline and the somatic gonadal tissue of the hermaphrodite gonad (Fig. 2).

A medial optical section through the hermaphrodite gonad shows that ETR-1 exhibits a diffuse, cytoplasmic staining throughout the entire hermaphrodite gonad (Fig. 2A–C). We also observed cytoplasmic expression of ETR-1 within both the female and male gametes (egg and sperm, respectively) (Fig. 2I–L, arrows indicates sperm). A superficial optical section of the proximal hermaphrodite gonad shows that ETR-1 is localized specifically to the gonadal sheath cell myofilaments. This result was confirmed by colocalization with an antibody against myosin heavy chain A (MHCA) (Fig. 2D–F) (Hubbard and Greenstein, 2000; Rose et al., 1997). Further confirmation of ETR-1 being expressed in the somatic gonadal cells emerges when imaging the surface of the distal gonad. ETR-1 exhibits a honeycomb pattern in the distal germ line that is consistent with the pattern observed by Hall et al. (1999) in their description of the individual somatic gonadal sheath cells via TEM and immunofluorescence studies (Fig. 2G–H) (Hall et al., 1999). To verify the specificity of the newly generated ETR-1 antibody, we show via western analysis that the antibody recognizes bands of the predicted molecular weights for the various ETR-1 splice isoforms, that a

subset of the bands observed in *etr-1(RNAi)* protein lysates are decreased in intensity compared to *control(RNAi)* animals, and that in dissected gonads from ETR-1-depleted animals the intensity of ETR-1 staining goes down compared to control depleted animals (Supplementary Fig. S3).

Analysis of embryos indicates early embryonic expression of ETR-1 that persists through the comma stage of embryonic development (Fig. 2M–N). In early embryos (1- to 16-cell stage), ETR-1 is diffusely cytoplasmic (Fig. 2N, arrowheads). In older embryos (> 32-cell), while there still remains some diffuse cytoplasmic ETR-1 staining, a majority of the ETR-1 is now nuclear (Fig. 2N, arrows). Both cytoplasmic and nuclear expression of CELF/Bruno family members has been previously reported in analysis of transfected mouse *Brunol1* into NIH 3T3 mouse embryonic fibroblast cells and HeLa cells stained for human CUGbp1 (Dev et al., 2007; Timchenko et al., 1996). This dynamic expression of ETR-1 is an area of future investigation.

### 3.4 Reduction of brood size upon ETR-1 depletion is not due to alterations in ovulation rates, overall gonad size, or germline mitotic index

Animals depleted of ETR-1 have a reduced brood size, however, the cause of this reduction is unknown. In determining brood size, we have counted the number of laid unfertilized eggs, arrested embryos, developing embryos and larvae. Thus embryonic lethality does not factor into our observed reduced brood. As such, we hypothesized three possibilities that might explain this reduction in brood phenotype: 1) reduced reproductive capacity (i.e. germ cell number or mitotic index); 2) decreased ovulation rates; or 3) reduced oocyte quality as a result of alterations in physiological germline apoptosis and/or a reduction in engulfment of apoptotic corpses (Andux and Ellis, 2008). This last possibility was suggested by Green et al., 2011 in which they observed the accumulation of germline cell corpses in ETR-1-depleted animals (Green et al., 2011). Our data shows that the mitotic index, ovulation rates, and gonad size are unchanged upon *etr-1(RNAi)*, however there is a difference in both oocyte size and germline apoptosis in ETR-1-depleted animals (Table 1, Figs. 3–5).

Germline proliferation can be calculated by determining the mitotic index within the proliferative zone of the gonad. The mitotic index is the ratio of the number of actively dividing cells, determined by staining with an antibody for phosphohistone H3 (pH3, a marker of mitosis) to the total number of cells as determined by staining with DAPI (Crittenden et al., 2006). There is no difference between the mitotic index observed in *control(RNAi)* animals versus *etr-1(RNAi)* animals (Table 1, 5.46 versus 4.86 respectively, p-value = 0.21).

Ovulation rate was determined by calculating the number of ovulations per hour. Through this method we determined that there was no difference in ovulation rate between *control(RNAi)* and *etr-1(RNAi)* animals. Animals treated with *control(RNAi)* exhibited an average of 3.98 ovulations per hour, while *etr-1(RNAi)* animals underwent an average of 4.04 ovulation per hour (Table 1). Similarly measurements of the length of the gonad, as determined by measuring the anterior gonad length and the length of the uterus, indicated no overall gonad size difference between *control(RNAi)* and *etr-1(RNAi)* animals (Table 1).

However, our observations suggested that the oocytes in *etr-1(RNAi)* animals might be smaller in area than those in *control(RNAi)* animals.

### 3.5 ETR-1 depletion results in smaller oocytes

Once oocytes become individualized, they continue to grow in size as they become more proximal in the germ line via the accumulation of a stockpile of nutrients, namely yolk (Grant and Hirsh, 1999; Greenstein, 2005; Hubbard and Greenstein, 2005). The yolk is synthesized in the intestine and then secreted into the pseudoceolomic cavity where it eventually undergoes receptor-mediated endocytosis into the growing oocytes (Grant and Hirsh, 1999; Hall et al., 1999; Kimble and Sharrock, 1983). Andux and Ellis (2008) showed that a decrease in oocyte size is correlated with a decrease in oocyte quality, with oocyte quality being measured as the percentage of eggs/embryos that died before hatching (Andux and Ellis, 2008).

To determine if oocyte size is altered upon RNAi depletion of ETR-1, we utilized DIC imaging to image oocytes in both *control(RNAi)* and *etr-1(RNAi)* hermaphrodites, and then used Nikon NIS-Elements software to determine the average area of individual oocytes ranging from the −1 to the −6 position. We observed via DIC that oocytes in *etr-1(RNAi)* gonads appeared physically smaller than in *control(RNAi)* gonads (Fig. 3A–B). Quantification of the average oocyte area of a single focal plane showed that at each oocyte position (−1 through the −6), the oocytes in ETR-1-depleted animals were smaller than oocytes in control-depleted animals (Fig. 3C). The largest difference in oocyte size was observed in the −1 oocyte, with a median area of 1087.9 $\mu m^2$ in *control(RNAi)* animals and 840.7 $\mu m^2$ in *etr-1(RNAi)* animals (Fig. 3C, p-value = 0.001). Thus it appears upon ETR-1 depletion, the oocytes are not able to accumulate as much nutrients as control-depleted animals.

### 3.6 ETR-1-depleted animals exhibit a significant increase in the number of germline apoptotic cell corpses

Physiological germline apoptosis is a natural feature of oogenesis that occurs just distal to the “loop region” or gonad bend where the germ cells exist in meiotic pachytene (Bailly and Gartner, 2013; Gartner et al., 2008; Lettre and Hengartner, 2006). More than half of all developing oocytes undergo programmed cell death, and this is hypothesized to occur in order to help maintain the integrity of the germ line by providing both space and cytoplasmic nutrients for the remaining germ cells to grow and survive (Conradt et al., 2016; Conradt and Xue, 2005; Gartner et al., 2008). Many of the core regulators of the physiological apoptotic pathway have been identified (for example, CED-3 and CED-4), however there still remains some uncertainty regarding the mechanism by which physiological germline apoptosis is initiated (Bailly and Gartner, 2013; Gartner et al., 2008; Gumienny et al., 1999). We determined the number of germline apoptotic cell corpses in *control(RNAi)* and *etr-1(RNAi)* treated animals by staining with acridine orange, a marker for apoptotic cells (Lant and Derry, 2014). Wild-type animals depleted of ETR-1 have a significant increase in the number of cell corpses staining positively for acridine orange within the gonad region just distal to the gonad loop compared to control-depleted animals (Fig. 4A–B). We quantified these numbers and show that germ lines depleted of ETR-1 have

2.8-fold more apoptotic cell corpses under our assay conditions (Fig. 4E, average apoptotic cells for wild-type strain: *control(RNAi)* = 3.9, *etr-1(RNAi)* = 11.0, p-value < 0.0001).

To ensure that the bodies observed were indeed apoptotic corpses, we utilized an established assay taking advantage of two strong mutations, *ced-3(n717)* and *ced-4(n1162)*, in pro-apoptotic genes that block almost all programmed cell death (Ellis and Horvitz, 1986; Gumienny et al., 1999; Yu et al., 2008; Yuan et al., 1993). Both *ced-3(n717)* and *ced-4(n1162)* were able to suppress the increased number of germline apoptotic cell corpses observed upon ETR-1 depletion. The average number of apoptotic cell corpses found in wild-type *etr-1(RNAi)* animals was 11.0 (Fig. 4E), compared to an average of 0 cell corpses observed in *ced-3(n717) etr-1(RNAi)* and *ced-4(n1162) etr-1(RNAi)* germ lines (data not shown). This indicates that the extra cell corpses we observe via acridine orange are generated by programmed cell death.

We utilized the somatic and germline RNAi defective strains to determine if the increased number of apoptotic cell corpses is due to a decrease in ETR-1 levels in the soma, the germ line or in both tissues (Fig. 4E and Supplementary Fig. S4). A significant increase in the average number of apoptotic cell corpses is observed upon depletion of ETR-1 in both the somatic RNAi defective strain [*rrf-1(pk1417)*] and in the germline RNAi defective strain [*ppw-1(pk1425)*] (Fig. 4E; *ppw-1(pk1425) control(RNAi)* = 3.9 apoptotic cells, *ppw-1(pk1425) etr-1(RNAi)* = 6.0 apoptotic cells, p-value = 0.001; *rrf-1(pk1417) control(RNAi)* = 7.3 apoptotic cells, *rrf-1(pk1417) etr-1(RNAi)* = 12.3 apoptotic cells, p-value < 0.0001). Interestingly, under our assay conditions the *rrf-1(pk1417)* animals fed *control(RNAi)* exhibited an increased number of apoptotic cell corpses compared to the similarly treated wild-type animals (Fig. 4E). This observation has not been previously reported for *rrf-1(pk1417)* and we have not investigated it further. All together this data suggests that ETR-1 plays a role both in the soma and the germ line to regulate either the process of physiological germline apoptosis or the engulfment of existing apoptotic corpses (see below).

Once a germ cell undergoes apoptosis, the resulting cell corpse must be engulfed by the somatic sheath cells (Gumienny et al., 1999). Engulfment and quick degradation of dying cells is extremely important to prevent the apoptotic signals and any harmful contents from spreading to neighboring, surviving cells (Bailly and Gartner, 2013; Savill and Fadok, 2000; Yu et al., 2008). There are currently three engulfment pathways that are involved in removal of dying cells in C. elegans: CED-1/CED-6/CED-7, CED-2/CED-5/CED-12, and PAT-2/PAT-3 (Conradt et al., 2016). CED-1 has been previously shown to localize to the extending pseudopods of engulfing cells and is an indicator for early apoptotic cells before and during engulfment (Gartner et al., 2008; Schumacher et al., 2005; Zhou et al., 2001). We utilized strain MD701 expressing a functional CED-1::GFP fusion protein in the gonadal sheath cells to determine if there were differences between the number of early apoptotic cells upon ETR-1 depletion (Zhou et al., 2001). As previously shown, MD701 exhibited CED-1::GFP expression strongly throughout the gonadal sheath, and we were able to observe CED-1::GFP positive cells within the gonad in both control- and ETR-1-depleted animals (Fig. 4C–D). Similar to the results for acridine orange, the gonads of animals depleted of ETR-1 have an increase (1.4-fold) in the number of CED-1::GFP positive cells compared to

control-depleted animals (Fig. 4F, average early apoptotic cells: *control(RNAi)* = 8.4, *etr-1(RNAi)* = 11.9, p-value < 0.0001). Combined this data shows that the number of germline apoptotic cells is increased upon ETR-1 depletion, however the mechanism by which this is occurring remains unknown.

### 3.7 Loss of ETR-1 results in apoptotic germ cell corpses that are not completely engulfed

Multiple factors, such as the rates of germ cell proliferation and apoptotic corpse-engulfment, have been reported to influence the number of apoptotic germ cells observed (Bailly and Gartner, 2013). We have already shown that the rate of germ cell proliferation, as determined by calculating mitotic index, in *control(RNAi)* and *etr-1(RNAi)* animals does not differ (Table 1). As such we turned to look at whether the process of engulfment of the dying cell and cell corpse removal was affected in *etr-1(RNAi)* animals. We utilized transmission electron microscopy (TEM) to analyze whether there were any ultra-structural differences in the gonads of animals depleted of a control gene or *etr-1*.

In control gonads, healthy germ cells were identifiable throughout the gonad, including the distal-most mitotic region, the transition zone, the meiotic zone, and within the gonad loop (Fig. 5A, n = 7). However of the multiple TEM images taken from 7 different control-treated animals, we were unable to capture any TEM images of apoptotic germ cells in the region distal to the gonad loop where physiological apoptosis is known to occur (Bailly and Gartner, 2013; Gumienny et al., 1999). This result is not surprising because it is very challenging to catch an apoptotic cell by TEM due to how quickly the dying cells are typically engulfed and removed (David Hall, personal observations). Conversely, in all *etr-1(RNAi)* animals imaged both healthy and apoptotic germ cells were observed in the gonad region immediately distal to the loop (Fig. 5B, n = 3). Quantification of the number of apoptotic germ cells observed ranged from 1 to 3 apoptotic cells per ETR-1-depleted gonad (average number of apoptotic cells by TEM: *control(RNAi)* = 0 ± 0, *etr-1(RNAi)* = 2.3 ± 1.2; p-value = 0.0004).

Examining the apoptotic germ cells within *etr-1(RNAi)* animals at a higher magnification provided additional information about the dying cells. Our TEM data indicates failure of the gonadal sheath cells to completely engulf apoptotic germ cells (Fig. 5C–D, gonadal sheath pseudocolored pink). Five out of the 7 apoptotic cells observed in *etr-1(RNAi)* animals show a failure of the gonadal sheath to engulf the dying cells (Fig. 5C). However, engulfment is possible as evident by the fact that within all our samples we observed a total of two apoptotic cells that were completely engulfed by the sheath (Fig. 5D, one engulfed apoptotic cell shown). This suggests that upon reduction of ETR-1, the gonadal sheath is still capable of engulfing dying cells, yet does so either at a much lower frequency and/or slower rate.

Finally, several TEM images indicated increased yolk accumulation in the pseudocoelom of ETR-1-depleted animals compared to controls (data not shown). This observation is consistent with either a defect(s) in the oocytes or the gonadal sheath cells or both. A build up of yolk in the pseudocoelom can be the result of a lack of healthy oocytes ready to receive yolk, or defects in the proximal gonadal sheath pores inhibiting the passage of yolk from the intestine into the oocytes (Herndon et al., 2002; Kimble and Sharrock, 1983). Previous studies reported that yolk uptake is very efficient with a majority of the yolk being

observed within the hermaphrodite intestine or oocytes, and only minor quantities of yolk observed within the sheath cells or pseudocoelom (Hall et al., 1999). We are currently further characterizing and quantifying this phenotype to determine whether this observation is a result of the depletion of ETR-1 in the somatic sheath pores or the oocytes.

### 3.8 Depletion of CED-1 suppresses both the ETR-1-depletion fertility defects and the increased apoptotic cell corpse phenotype

After observing defects in engulfment, we wanted to further investigate ETR-1's potential role in the engulfment of apoptotic germ cells. We began by asking whether ETR-1 was involved in the CED-1 engulfment pathway mentioned above (Conradt et al., 2016). Accordingly, we obtained a *ced-1* engulfment mutant, *ced-1(e1735)*, that had been previously characterized as defective in apoptotic cell engulfment (Hedgecock et al., 1983). We depleted ETR-1 by RNAi feeding in the *ced-1(e1735)* mutants, and asked whether the average brood of the treated animals was affected compared to that of wild-type animals. The *ced-1(e1735)* animals treated with a *control(RNAi)* have an average brood that is similar to that observed in wild-type animals fed the same control RNAi construct (Fig. 6A, compare *control(RNAi)* bars). However, when we compared broods resulting from either ETR-1-depleted wild-type or *ced-1(e1735)* animals we observed a significant increase in the brood of the treated *ced-1* mutants (Fig. 6A; compare *etr-1(RNAi)* bars; average brood: wild-type = 118 ± 3.1, *ced-1(e1735)* = 147 ± 6.7; p-value < 0.0001; N > 47). The average brood of *ced-1(e1735) etr-1(RNAi)* animals is not significantly different from that observed in *ced-1(e1735) control(RNAi)* animals (Fig. 6A; compare grey bars; average brood: *control(RNAi)* = 163 ± 6.2, *etr-1(RNAi)* = 147 ± 6.7; p-value = 0.08; N > 47). We ensured that the *ced-1(e1735)* animals were responsive to RNAi by subjecting mutant animals to *wee-1.3(RNAi)* and observing the reported sterility phenotype (Fig. 6A, compare *wee-1.3(RNAi)* bars). Finally, 76% of the resulting brood from *ced-1(e1735) etr-1(RNAi)* animals arrest at the PAT stage, which is not statistically different from the 87% of PAT arrested embryos observed in wild-type *etr-1(RNAi)* animals (Fig. 1B and data not shown). This supports the fact that *etr-1(RNAi)* is functioning in the *ced-1* mutant animals to reduce the levels of ETR-1. It is worthwhile to note again that there is an *etr-1* deletion allele, however we cannot currently test the potential interaction between *ced-1* and *etr-1* by generating a double mutant of both because the available iallele is homozygous lethal.

We then compared the average number of apoptotic cell corpses observed upon RNAi depletion of ETR-1 with the number of cell corpses observed upon RNAi depletion of CED-1 (Fig. 6B). It was necessary to do this experiment via RNAi depletion because it is known that engulfment mutants, such as CED-1, cannot be labeled with acridine orange (Gartner et al., 2008; Lant and Derry, 2014). Similar to published data we observe an increase number of germline apoptotic cell corpses upon depletion of CED-1 when compared to control-depleted animals (Fig. 6B; average apoptotic cell corpses: *control(RNAi)* = 5.2 ± 0.4; *ced-1(RNAi)* = 6.9 ± 0.6; p-value = 0.02). However this number is significantly lower than what we observe upon ETR-1 depletion (Fig. 6B; average apoptotic cell corpses: *ced-1(RNAi)* = 6.9 ± 0.6; *etr-1(RNAi)* = 10.1 ± 0.6; p-value = 0.0004). When we co-deplete both ETR-1 and CED-1, we see a suppression of the number of increased apoptotic cell corpses observed upon single depletion of ETR-1 (Fig. 6B;

average apoptotic cell corpses: *etr-1(RNAi)* = 10.1 ± 0.6; *etr-1(RNAi) ced-1(RNAi)* = 6.8 ± 0.4; p-value < 0.0001). The number of apoptotic cell corpses in the gonads of *etr-1(RNAi) ced-1(RNAi)* animals is not significantly different from the number observed in the gonads of *ced-1(RNAi)* animals (Fig. 6B; average apoptotic cell corpses: *ced-1(RNAi)* = 6.9 ± 0.6; *etr-1(RNAi) ced-1(RNAi)* = 6.8 ± 0.4; p-value = 0.8). We verified that ETR-1 was reduced upon the double RNAi treatment by quantifying the percentage of PAT embryos in the brood (Supplementary Fig. S5). 70% of the resulting brood from *etr-1(RNAi) ced-1(RNAi)* animals arrest at the PAT stage, which is not statistically different from the 87% of PAT arrested embryos observed in wild-type *etr-1(RNAi)* animals (Fig. S5; p-value = 0.26). Taken together, these observations suggest that ETR-1 and CED-1 are functioning together in the same genetic pathway to promote proper engulfment of apoptotic germ cell corpses. If ETR-1 and CED-1 functioned in parallel pathways, one would expect enhancement of the engulfment defect and more cell corpses due to the additive effect of the double depletion, as has been reported for CED-1 and PAT-2 (Hsieh et al., 2012).

## 4. Discussion

The *C. elegans* ETR-1 protein has been regarded in the past as a muscle-specific RNA-binding protein (Milne and Hodgkin, 1999). Embryos from hermaphrodites treated with *etr-1(RNAi)* were shown to arrest at a very specific developmental time point, the two-fold stage, indicative of a failure in muscle elongation. In addition, further confirmation of a muscle role emerged when analysis of an ETR-1 transcriptional fusion reporter revealed muscle-specific expression. However, our lab had evidence supporting a reproductive role for ETR-1 when this gene emerged in a screen looking for candidates that could suppress the well-characterized WEE-1.3-depletion infertility phenotype (Allen et al., 2014). The studies presented in this paper demonstrate that ETR-1 plays a role during *C. elegans* oogenesis, and that ETR-1 is required in both the somatic gonad and the germ line in order to ensure an animal's full reproductive capacity. Additionally, we have identified a novel role for ETR-1 during physiological germline apoptosis in corpse cell engulfment.

### 4.1 Complexity of the ETR-1 genomic locus

The ETR-1 genomic locus is very complex and is currently annotated to consist of 19 predicted splice isoforms and one predicted non-coding transcript (WormBase: etr-1, www.wormbase.org). In the most recent curation, the locus exhibits multiple exon skipping events and alternative frame usage (for example, as observed for Isoforms P, Q, and R; see Supplementary Fig. S1). Intriguingly, one can notice an exclusivity of exons 8 and 10, in that isoforms either utilize exon 8, exon 10, or neither, but that none of the 19 isoforms consist of both exons 8 and 10 (Supplementary Fig. S1). Since it is known that isoforms resulting from alternative splicing can have distinct spatial specialization in organisms, one model as to why there are multiple ETR-1 isoforms is that different isoforms are required for disparate tissue and/or cellular processes (Gunning et al., 2005; Neidt et al., 2009). For example, a muscle function versus a neuronal function versus a reproductive function. This speculation is strengthened by the fact that in most organisms the CELF/Bruno protein family typically consists of multiple members with identifiable roles in the nervous system, heart, muscle, and reproductive tissues (Barreau et al., 2006; Dasgupta and Ladd, 2012). However, in *C.*

*elegans* there are only two members of this protein family, ETR-1 and UNC-75. Hence it is possible that the multiple isoforms of ETR-1 have arisen to compensate for the lack of protein members capable of playing the diverse functional roles characteristic of the CELF/Bruno family. Notably, UNC-75 has four protein isoforms and, as mentioned above, has a neuron specific role (Loria et al., 2003; WormBase: unc-75, www.wormbase.org). It will be interesting in the future to investigate any tissue specificity resulting from the inclusion of specific exons within particular ETR-1 isoforms.

Our alignment of all the ETR-1 protein isoforms with the closest human (CUGBP1) and *Drosophila* homologues (BRUNOL-2 and ELAV) confirms the presence of three RRMs (RRM1-3) in the largest ETR-1 isoforms. The highest evolutionary conservation is found within the third RRM (RRM3), which is present in all 19 isoforms (Supplementary Figs. S1 and S2). However, it is worthwhile to note that there is in fact a variation in the number of RRMs that individual ETR-1 isoforms contain. Six isoforms (A, D, E, F, G, and L) possess all three RRMs, three isoforms (M, N, and O) contain just RRM2 and RRM3, three isoforms (P, Q, and R) contain part of RRM2 and all of RRM3, while 7 isoforms (B, S, T, U, V, W, and X) only contain RRM3. Although all RRMs are thought to be involved in RNA binding, previous studies in other systems suggest that RRM3 increases the binding strength of an RBP to its RNA targets, while RRM1 and RRM2 cooperatively provide a large surface area for binding within the same RNA target molecule (Auweter et al., 2006; Tsuda et al., 2009). Those ETR-1 isoforms with multiple RRMs might thus be capable of binding different RNA targets than isoforms that possess just the one RRM3. Generating targeted mutations and/or substitutions in the two highly conserved RNP sequence stretches within each individual RRM (RNP1 and RNP2, see Supplementary Fig. S2) might assist in elucidating any potential RRM-specific mRNA targets.

While the isoforms obviously differ in their coding sequences, it is also worthwhile to note that there is significant variation in the non-coding exons present within the various isoforms (see grey regions in Supplementary Fig. S1). It is well acknowledged that the non-coding 5′ and 3′ untranslated regions (UTRs) of a gene serve varying regulatory functions (Mignone et al., 2002). In fact, many *C. elegans* laboratories have published studies indicating the inclusion of a gene's endogenous 5′ and 3′ UTR regions is important for proper expression when generating transgenic animals (Merritt et al., 2008; Merritt and Seydoux, 2010). Other RBPs could potentially be binding the unique 5′UTRs present within individual *etr-1* mRNA transcript sequences, and regulating the stability and/or translation of that transcript thereby making those mRNA transcripts specific to certain locations within the animal. Thus, elucidating the similarities and differences of expression pattern among the various ETR-1 isoforms will be an important area of future study. With CRISPR/Cas9 endogenous genome editing it will be possible to tag specific exons and begin to address this important question.

### 4.2 ETR-1 is required for full reproductive potential of hermaphrodites

While ETR-1 has previously been reported as involved in muscle development, we have identified novel roles for the ETR-1 protein both within the germ line and the somatic cells of the gonad. We show that depletion of ETR-1 via RNAi in wild-type hermaphrodite

animals results in a 32% decrease in fertility (Fig. 1A). While this is only a moderate decrease in the reproductive ability of ETR-1-depleted animals, it is sufficient to inform us that there is a functional requirement for ETR-1 in *C. elegans* reproduction. As our brood analysis was conducted by counting all progeny of the treated animals, including those that are embryonically arrested, the lower brood size is not due to the strong embryonic lethality known to occur upon *etr-1(RNAi)* treatment (Milne and Hodgkin, 1999). Rather our data implies that there is a role for ETR-1 in the *C. elegans* germ line that results in ETR-1-depleted animals having reduced fertility compared to control-depleted animals.

Additionally, there is a requirement of ETR-1 in both the somatic tissue and the germ line to ensure the full reproductive capability of the animal as evident by the RNAi experiments conducted in somatic RNAi deficient and germline RNAi deficient animals (Fig. 1A). When ETR-1 is only depleted in the germ line there is a small (18%), but significant, decrease in fertility. Similarly when ETR-1 is only depleted in the somatic tissue of animals, there is again a small (18%) but significant fertility decrease. We thus propose that ETR-1 is necessary in both the soma and the germ line to ensure normal fertility levels, and that it is the additive effects of ETR-1 depletion in both the germ line and the somatic tissue that results in the overall fertility reduction.

The fertility data is further supported by the identification that ETR-1 is expressed in the somatic gonadal sheath cells encasing the germ line, and within the male and female germ cells (Fig. 2). The ETR-1 antibody generated in this study is the first to show ETR-1 expression in the gonad. Previous analysis of ETR-1 expression only identified muscle-specific expression, but did not specifically identify gonadal sheath expression (Milne and Hodgkin, 1999). This difference in expression analysis can be explained by the fact that the Milne and Hodgkin's study was conducted utilizing a transgenic animal containing a non-integrated, extrachromosomal array of an ETR-1 transcriptional fusion reporter (Milne and Hodgkin, 1999). It is now known that the germ line is exceptionally adept at silencing multi-copy transgenes, and hence it is not surprising that no germline expression was observed for this particular ETR-1 reporter (Kelly et al., 1997; Merritt and Seydoux, 2010).

The expression of ETR-1 in the gonadal sheath cells is intriguing due to the previously identified roles played by the sheath cells and the phenotypes observed upon ETR-1 depletion (Figs. 1 and 3–5). It is known that the more distal sheath cell pairs 2 and 3 play a role in engulfing apoptotic germ cells, while the proximal sheath cells (pairs 4 and 5) are required for regulating oocyte meiotic maturation and ovulation (Greenstein et al., 1994; Lints and Hall, 2009b; Rose et al., 1997). Additionally, sheath cell pair 5 is responsible for providing sheath pores that allow yolk uptake from the pseudocoelom to the growing oocyte (Hall et al., 1999). Upon ETR-1 depletion, we observed both a decrease in proximal oocyte size and an increase in apoptotic germ cell corpses (Figs. 3 and 4). The decrease in oocyte size can be attributed to a failure to appropriately uptake yolk through sheath cell pair 5 as part of the maturation process, while we propose increased apoptotic corpses is related to a failure in the normal functioning of sheath cell pairs 2 and 3 to engulf and remove the corpses (Figs. 3 and 4 and discussion below). Both a decrease in oocyte size and increased apoptosis have been shown previously to result in poor quality oocytes that have an increased rate of embryonic lethality after fertilization (Andux and Ellis, 2008).

Additionally, there is a connection between ETR-1 and oocyte meiotic maturation in that ETR-1 depletion is able to suppress a precocious oocyte maturation defect observed upon WEE-1.3 depletion (Fig. 1A). Thus we propose that ETR-1 functions in sheath cells 2 and 3 to engulf apoptotic corpses and sheath cells 4 and 5 to ensure proper yolk uptake and the generation of high quality oocytes. As we observed no difference in ovulation rates between control-depleted and ETR-1-depleted animals we do not believe that ETR-1 plays a role in ovulation (Table 1).

The role of ETR-1 in oocyte maturation was further investigated by asking the question in which tissue, somatic or germ line, did ETR-1 have to be depleted in order to suppress the WEE-1.3-depletion infertility phenotype. Co-depletion of ETR-1 and WEE-1.3 in *rrf-1(pk1417)* somatic RNAi defective animals failed to suppress the infertility observed upon WEE-1.3-depletion and upon co-depletion of ETR-1 and WEE-1.3 in wild-type animals (Fig. 1A). This leads us to propose that the suppression is dependent on a reduction of ETR-1 levels in the gonadal sheath cells. However, the mechanism by which ETR-1 depletion can suppress the *wee-1.3(RNAi)* infertility still remains an active area of investigation. Importantly, neither suppression of WEE-1.3-depleted infertility nor a reduction in fertility occurs when ETR-1's paralog, UNC-75, is depleted (data not shown). This adds further support to our hypothesis that ETR-1 is the only CELF/Bruno family member within *C. elegans* that functions in the reproductive tissues.

Why might ETR-1 be important for oocyte meiotic maturation? Many laboratories have established that translation regulation is critical for meiotic maturation (Kim et al., 2013; Richter and Lasko, 2011). As an RNA-binding protein, ETR-1 has the potential to be able to regulate gene expression at the level of translation. The cytoplasmic ETR-1 expression that we observe in the oocytes places ETR-1 in the right location to be regulating the translation of its targets. To determine if this is in fact occurring, future studies are needed to identify the specific mRNA targets of ETR-1, and establish whether these targets are differentially regulated in the presence and absence of ETR-1 during meiotic maturation.

### 4.3 ETR-1 is required for engulfment of apoptotic cell corpses

Loss of ETR-1 via RNAi depletion results in a significant increase in the number of germline apoptotic cells (Figs. 4–6). ETR-1 is not the first RBP implicated in physiological germ cell apoptosis, as depletion of the RBP CAR-1 has also been reported to increase germline apoptosis (Boag et al., 2005). The increase in apoptotic cells was confirmed through multiple independent experiments: first by examining the number of early CED-1::GFP positive apoptotic cells (Fig. 4C–D,F), second by determining the number of committed apoptotic cells by acridine orange staining (Fig. 4A–B,E), and third through TEM analysis (Fig. 5B). An increased number of acridine orange positive cells, or apoptotic cells, was observed in both the somatic and germline defective RNAi strains (Fig. 4E and Supplementary Fig. S4). This suggests that ETR-1 is needed in both the germ line and soma for an aspect of normal physiological germline apoptosis and/or engulfment. It is conceivable that depletion of only germline ETR-1 in the *rrf-1(pk1417)* somatic RNAi defective animals results in an increased number of germ cells undergoing apoptosis or results in defective apoptotic germ cell signaling for their timely engulfment/removal.

Meanwhile, depletion of somatic ETR-1 in the *ppw-1(pk1425)* germline RNAi defective strain might possibly result in a defective gonadal sheath that cannot function properly in the process of engulfment of apoptotic cell corpses. Our TEM analysis provides supporting evidence that the gonadal sheath in ETR-1-depleted animals is defective in engulfment based on the observation that a majority of the apoptotic cells in ETR-1-depleted animals are not completely engulfed by the sheath cells, however full engulfment can occur (Fig. 5B–D). Currently we are unable to discriminate if depletion of ETR-1 results in increased rates of apoptosis or a failure to properly engulf and remove apoptotic corpses. Future studies will be aimed at delineating between these two potential hypotheses. However the observed incomplete engulfment is indicative of defects in gonadal sheath cell function, which is also supported by the increased yolk accumulation observed in the pseudocoelom (data not shown). Also, our strong expression data of ETR-1 in the gonadal sheath suggests a role for ETR-1 in the sheath (Fig. 2D–H).

Interestingly, the gonads of ETR-1-depleted animals have the same number of early apoptotic cells, as evident by CED-1::GFP staining, and committed apoptotic cells, as evident by acridine orange staining (Fig. 4E–F). This is unlike what we observe in *control(RNAi)* animals where the average number of early apoptotic bodies is higher than the number of committed apoptotic bodies (early = 8.4, committed = 3.9). The observations in control treated animals is in agreement with what has been previously reported that not every CED-1::GFP surrounded cell will continue on to form an apoptotic corpse (Craig et al., 2012; Gartner et al., 2008). This suggests that once cells in ETR-1-depleted germ lines begin the apoptotic process, there is a higher likelihood that the cells will progress completely through apoptosis and become apoptotic cell corpses.

Having observed a defect in engulfment, we started to investigate genes known to be involved in the process of engulfment. We discovered that co-depletion of CED-1 with ETR-1 was able to suppress both the reduced brood size and the increased number of apoptotic cells observed in single ETR-1-depleted animals (Fig. 6). This lack of enhancement of both phenotypes suggests that ETR-1 acts in the same genetic pathway as CED-1. Further support for this is emerging from preliminary results within the laboratory that indicate that co-depletion of ETR-1 and CED-2, a member of an engulfment pathway distinct from the CED-1 pathway, does not have the suppressive effect observed by CED-1 (data not shown). This potentially suggests that ETR-1 and CED-2 might be acting in separate pathways. Further experimentation will be necessary to either place ETR-1 into the CED-1/CED-6/CED-7 engulfment pathway, into one of the other two known engulfment pathways (CED-2/CED-5/CED-12 or PAT-2/PAT-3), or in its own novel engulfment pathway. Currently we cannot rule out the possibility that in the co-depletion situations, when both *ced-1* and *etr-1* double stranded RNAs are present, that the effectiveness of the RNAi towards each gene might be mutually weakened.

Finally, according to data available on WormBase of the 8 genes currently known to be involved in the three different engulfment pathways (CED-1, CED-6, CED-7, CED-2, CED-5, CED-12, PAT-2, and PAT-3), only one (CED-12) has been reported to have a reduced brood size (Gumienny et al., 2001; Harris et al., 2010). This is suggestive that failure to properly engulf apoptotic corpses does not normally result in decreased fertility.

Interestingly, the average number of apoptotic cell corpses we observed in the *ced-1(RNAi)* treated animals (6.9) is similar to the average number reported for *ced-12* mutant animals (6.1), however the *ced-12* mutants were reported to have a 41% reduction in total brood compared to wild-type animals (Gumienny et al., 2001). We found significantly more apoptotic cell corpses in *etr-1(RNAi)* treated animals (an average of 10.1, Fig. 6B), yet this only resulted in a 32% reduction in 24 h brood compared to control treated animals (Fig. 6A). As our experiments were conducted utilizing RNAi depletion, it is possible that we are not fully knocking down ETR-1, hence the reason we observe more apoptotic cells but less of a reduction in brood size compared to what is observed in the *ced-12* mutant studies. Also, Gumienny et al. calculated a lifetime total brood of their mutant animals, while we were only calculating a 24 h brood, hence we may be underrepresenting the reduction in brood (Gumienny et al., 2001). Combining the apoptotic data with the observed expression pattern of ETR-1, we hypothesize that the reduction in brood size in animals depleted of ETR-1 is due to the increase in number of germline apoptotic cell corpses resulting in the generation of lower quality oocytes, and the requirement of ETR-1 within the gonadal sheath cells for timely engulfment and removal of the cell corpses.

### 4.4 ETR-1 exhibits variation in spatial expression in embryos

Analysis of embryonic ETR-1 expression denoted a change in subcellular localization from diffusely cytoplasmic in young embryos (up to the 16-cell stage) to mostly nuclear in older embryos (> 32-cell stage) (Fig. 2M–N). Similar to other RBPs, the CELF/Bruno proteins have been shown to play distinct nuclear roles in alternative splicing and RNA editing (Barreau et al., 2006; Dasgupta and Ladd, 2012). This is in addition to their more well-known cytoplasmic roles in dead-enylation, mRNA stability, and translational regulation (Dasgupta and Ladd, 2012). The nuclear expression during later embryonic development is thus most likely indicative of a shift towards ETR-1 being required to appropriately regulate alternative splicing of its target mRNAs during specific developmental timepoints. We hypothesize that some of the embryonic targets are muscle genes, and this would explain why ETR-1-depleted embryos exhibit a failure in muscle elongation and arrest with a PAT phenotype (Milne and Hodgkin, 1999). In the future studying how the disparate functional activities of ETR-1 in the cytoplasm and the nucleus are coordinated will be an interesting area of study, and provide us with new information regarding this important, highly conserved protein family.

## 5. Conclusions

Our research provides several lines of evidence to suggest that ETR-1 has functional roles during reproduction both in the germ line and the somatic tissue of the gonad. The loss of ETR-1 results in a decreased reproductive potential for the affected animal. This reproductive role is novel and previously unappreciated for ETR-1. Implicating ETR-1 in the engulfment of germline apoptotic cells adds a new player to this important cellular pathway by which more than 50% of germ cells are programmed to die and are eventually removed from the gonad. Future studies on ETR-1 are required to delve into the intricacies associated with this complex genomic locus and elucidate potential isoform-specific functions. Finally, one key question that remains is what are the RNA targets of ETR-1? Based on our reported

results, we speculate that some of the RNA targets of ETR-1 might potentially be the *ced* genes themselves and/or meiotic cell cycle genes in the same pathway as WEE-1.3. Establishing a direct relationship between ETR-1 and specific RNA targets will help in elucidating the mechanism by which ETR-1 affects physiological germ cell apoptosis, and ultimately help us determine how co-depletion of ETR-1 and WEE-1.3 results in suppression of the WEE-1.3-depletion infertility.

## Supplementary Material

Refer to Web version on PubMed Central for supplementary material.

## Acknowledgments

We thank the Anderson lab, Duttaroy lab, and Robinson lab for sharing equipment and reagents; Lourds Michelle Fernando for technical assistance and comments on the manuscript; members of the Baltimore Worm Club and Erin Cram for helpful discussions; and WormBase. The monoclonal myosin heavy chain A (5–6) antibody developed by Henry Epstein was obtained from the Developmental Studies Hybridoma Bank, created by the NICHD of the NIH and maintained at The University of Iowa, Department of Biology, Iowa City, IA 52242. Some nematode strains used in this work were provided by the CGC, which is funded by NIH Office of Research Infrastructure Programs (P40 OD010440). The *etr-1(tm6221)* knockout was generated by the National Bioresource Project in Tokyo, Japan which is part of the International *C. elegans* Knockout Consortium. The spinning disk confocal microscope was acquired through a Department of Defense HBCU/MI Equipment/Instrumentation Grant (#64684-RT-REP) to A. Allen. R. Boateng was supported in part by a Howard University Graduate Assistantship through the HU Graduate School. A. Allen was supported by Howard University start-up funds, a mini-grant award from Sonya Smith's NSF Howard University ADVANCE-IT grant (Award #1208880), and NIH 1R15HD084253-01A1 to A.K.A.. A. Golden was supported by the Intramural Research Program of the National Institutes of Health (NIH), National Institute of Diabetes and Digestive and Kidney Diseases. D.H. Hall and K.C. Nguyen were supported by NIH OD 010943 to D.H.H..

## Appendix A. Supporting information

Supplementary data associated with this article can be found in the online version at doi: 10.1016/j.ydbio.2017.06.015.

## References

Allen AK, Nesmith JE, Golden A. An RNAi-based suppressor screen identifies interactors of the Myt1 ortholog of Caenorhabditis elegans. G3 (Bethesda). 2014; 4:2329–2343. http://dx.doi.org/10.1534/g3.114.013649. [PubMed: 25298536]

Andux S, Ellis RE. Apoptosis maintains oocyte quality in aging Caenorhabditis elegans females. PLoS Genet. 2008; 4 http://dx.doi.org/10.1371/journal.pgen.1000295.

Auweter SD, Oberstrass FC, Allain FHT. Sequence-specific binding of single-stranded RNA: is there a code for recognition? Nucleic Acids Res. 2006; 34:4943–4959. http://dx.doi.org/10.1093/nar/gkl620. [PubMed: 16982642]

Bailly A, Gartner A. Germ cell apoptosis and DNA damage responses. Adv Exp Med Biol. 2013; 757:249–276. http://dx.doi.org/10.1007/978-1-4614-4015-4-9. [PubMed: 22872480]

Barreau C, Paillard L, Mereau A, Osborne HB. Mammalian CELF/Bruno-like RNA-binding proteins: molecular characteristics and biological functions. Biochimie. 2006; 88:515–525. http://dx.doi.org/10.1016/j.biochi.2005.10.011. [PubMed: 16480813]

Boag PR, Nakamura A, Blackwell TK. A conserved RNA-protein complex component involved in physiological germline apoptosis regulation in C. elegans. Development. 2005; 132:4975–4986. http://dx.doi.org/10.1242/dev.02060. [PubMed: 16221731]

Brenner S. The genetics of Caenorhabditis elegans. Genetics. 1974; 77:71–94. [PubMed: 4366476]

C. elegans Deletion Mutant Consortium. Large-scale screening for targeted knockouts in the Caenorhabditis elegans genome. G3 (Bethesda). 2012; 2:1415–1425. http://dx.doi.org/10.1534/g3.112.003830. [PubMed: 23173093]

Castrillon DH, Gonczy P, Alexander S, Rawson R, Eberhart CG, Viswanathan S, DiNardo S, Wasserman SA. Toward a molecular genetic analysis of spermatogenesis in Drosophila melanogaster: characterization of male-sterile mutants generated by single P element mutagenesis. Genetics. 1993; 135:489–505. [PubMed: 8244010]

Ceron J, Rual JF, Chandra A, Dupuy D, Vidal M, van den Heuvel S. Large-scale RNAi screens identify novel genes that interact with the *C. elegans* retinoblastoma pathway as well as splicing-related components with synMuv B activity. BMC Dev Biol. 2007; 7:30. http://dx.doi.org/10.1186/1471-213X-7-30. [PubMed: 17417969]

Chen L, Liu Z, Zhou B, Wei C, Zhou Y, Rosenfeld MG, Fu XD, Chisholm AD, Jin Y. CELF RNA binding proteins promote axon regeneration in *C. elegans* and mammals through alternative splicing of Syntaxins. Elife. 2016; 5:e16072. http://dx.doi.org/10.7554/eLife.16072. [PubMed: 27253061]

Cléry, A., Blatter, M., Allain, FHT. RNA recognition motifs: boring? Not quite. Curr Opin Struct Biol. 2008. http://dx.doi.org/10.1016/j.sbi.2008.04.002

Colegrove-Otero LJ, Minshall N, Standart N. RNA-binding proteins in early development. Crit Rev Biochem Mol Biol. 2005; 40:21–73. http://dx.doi.org/10.1080/10409230590918612. [PubMed: 15804624]

Conradt B, Wu YC, Xue D. Programmed cell death during Caenorhabditis elegans development. Genetics. 2016; 203 (1533 LP-1562).

Conradt, B., Xue, D. Programmed cell death; WormBook. 2005. p. 1-13.http://dx.doi.org/10.1895/wormbook.1.32.1

Corsi AK, Wightman B, Chalfie M. A transparent window into biology: a primer on Caenorhabditis elegans. Genetics. 2015; 200:387–407. http://dx.doi.org/10.1534/genetics.115.176099. [PubMed: 26088431]

Craig AL, Moser SC, Bailly AP, Gartner A. Methods for studying the DNA damage response in the Caenorhabdatis elegans germ line. Methods Cell Biol. 2012; 107:321–352. http://dx.doi.org/10.1016/B978-0-12-394620-1.00011-4. [PubMed: 22226529]

Crittenden SL, Leonhard KA, Byrd DT, Kimble J. Cellular analyses of the mitotic region in the Caenorhabditis elegans adult germ line. Mol Biol Cell. 2006; 17:3051–3061. http://dx.doi.org/10.1091/mbc.E06-03-0170. [PubMed: 16672375]

Dasgupta T, Ladd AN. The importance of CELF control: Molecular and biological roles of the CUG-BP, Elav-like family of RNA-binding proteins. Wiley Interdiscip Rev RNA. 2012; 3:104–121. http://dx.doi.org/10.1002/wrna.107. [PubMed: 22180311]

Detwiler MR, Reuben M, Li X, Rogers E, Lin R. Two zinc finger proteins, OMA-1 and OMA-2, are redundantly required for oocyte maturation in C. elegans. Dev Cell. 2001; 1:187–199. [PubMed: 11702779]

Dev A, Nayernia K, Meins M, Adham I, Lacone F, Engel W. Mice deficient for RNA-binding protein Brunol1 show reduction of spermatogenesis but are fertile. Mol Reprod Dev. 2007; 74:1456–1464. http://dx.doi.org/10.1002/mrd.20742. [PubMed: 17393433]

Ellis HM, Horvitz HR. Genetic control of programmed cell death in the nematode C. elegans. Cell. 1986; 44:817–829. http://dx.doi.org/10.1016/0092-8674(86)90004-8. [PubMed: 3955651]

Gartner, A., Boag, PR., Blackwell, TK. Germline survival and apoptosis; WormBook. 2008. p. 1-20.http://dx.doi.org/10.1895/wormbook.1.145.1

Grant B, Hirsh D. Receptor-mediated endocytosis in the Caenorhabditis elegans oocyte. Mol Biol Cell. 1999; 10:4311–4326. [PubMed: 10588660]

Green RA, Kao HL, Audhya A, Arur S, Mayers JR, Fridolfsson HN, Schulman M, Schloissnig S, Niessen S, Laband K, Wang S, Starr DA, Hyman AA, Schedl T, Desai A, Piano F, Gunsalus KC, Oegema K. A high-resolution *C. elegans* essential gene network based on phenotypic profiling of a complex tissue. Cell. 2011; 145:470–482. http://dx.doi.org/10.1016/j.cell.2011.03.037. [PubMed: 21529718]

Greenstein, D. Control of oocyte meiotic maturation and fertilization; WormBook. 2005. p. 1-12.http://dx.doi.org/10.1895/wormbook.1.53.1

Greenstein D, Hird S, Plasterk RH, Andachi Y, Kohara Y, Wang B, Finney M, Ruvkun G. Targeted mutations in the Caenorhabditis elegans POU homeo box gene ceh-18 cause defects in oocyte cell cycle arrest, gonad migration, and epidermal differentiation. Genes Dev. 1994; 8:1935–1948. [PubMed: 7958868]

Gumienny TL, Brugnera E, Tosello-Trampont AC, Kinchen JM, Haney LB, Nishiwaki K, Walk SF, Nemergut ME, Macara IG, Francis R, Sched l T, Qin Y, Van Aelst L, Hengartner MO, Ravichandran KS. CED-12/ELMO, a novel member of the CrkII/Dock180/Rac pathway, is required for phagocytosis and cell migration. Cell. 2001; 107:27–41. http://dx.doi.org/10.1016/S0092-8674(01)00520-7. [PubMed: 11595183]

Gumienny TL, Lambie E, Hartwieg E, Horvitz HR, Hengartner MO. Genetic control of programmed cell death in the Caenorhabditis elegans hermaphrodite germline. Development. 1999; 126:1011–1022. [PubMed: 9927601]

Gunning, PW., Schevzov, G., Kee, AJ., Hardeman, EC. Tropomyosin isoforms: divining rods for actin cytoskeleton function. Trends Cell Biol. 2005. http://dx.doi.org/10.1016/j.tcb.2005.04.007

Hall DH, Winfrey VP, Blaeuer G, Hoffman LH, Furuta T, Rose KL, Hobert O, Greenstein D. Ultrastructural features of the adult hermaphrodite gonad of Caenorhabditis elegans: relations between the germ line and soma. Dev Biol. 1999; 212:101–123. http://dx.doi.org/10.1006/dbio.1999.9356. [PubMed: 10419689]

Harris TW, Antoshechkin I, Bieri T, Blasiar D, Chan J, Chen WJ, De La Cruz N, Davis P, Duesbury M, Fang R, Fernandes J, Han M, Kishore R, Lee R, Muller HM, Nakamura C, Ozersky P, Petcherski A, Rangarajan A, Rogers A, Schindelman G, Schwarz EM, Tuli MA, Van Auken K, Wang D, Wang X, Williams G, Yook K, Durbin R, Stein LD, Spieth J, Sternberg PW. WormBase: a comprehensive resource for nematode research. Nucleic Acids Res. 2010; 38 http://dx.doi.org/10.1093/nar/gkp952.

Hedgecock EM, Sulston JE, Thomson JN. Mutations affecting programmed cell deaths in the nematode Caenorhabditis elegans. Science. 1983; 80(220):1277–1279. http://dx.doi.org/10.1126/science.6857247.

Herndon, La, Schmeissner, PJ., Dudaronek, JM., Brown, Pa, Listner, KM., Sakano, Y., Paupard, MC., Hall, DH., Driscoll, M. Stochastic and genetic factors influence tissue-specific decline in ageing C. elegans. Nature. 2002; 419:808–814. http://dx.doi.org/10.1038/nature01135. [PubMed: 12397350]

Hsieh HH, Hsu TY, Jiang HS, Wu YC. Integrin alpha PAT-2/CDC-42 signaling is required for muscle-mediated clearance of apoptotic cells in Caenorhabditis elegans. PLoS Genet. 2012; 8 http://dx.doi.org/10.1371/journal.pgen.1002663.

Hubbard, EJA., Greenstein, D. Introduction to the germ line; WormBook. 2005. p. 1-4.http://dx.doi.org/10.1895/wormbook.1.18.1

Hubbard EJ, Greenstein D. The Caenorhabditis elegans gonad: a test tube for cell and developmental biology. Dev Dyn. 2000; 218:2–22. [PubMed: 10822256]

Kelly WG, Xu S, Montgomery MK, Fire A. Distinct requirements for somatic and germline expression of a generally expressed Caernorhabditis elegans gene. Genetics. 1997; 146:227–238. [PubMed: 9136012]

Kim S, Spike C, Greenstein D. Control of oocyte growth and meiotic maturation in C. elegans. Adv Exp Med Biol. 2013; 757 http://dx.doi.org/10.1007/978-1-4614-4015-4_10.

Kimble J, Sharrock WJ. Tissue-specific synthesis of yolk proteins in Caenorhabditis elegans. Dev Biol. 1983; 96:189–196. http://dx.doi.org/10.1016/0012-1606(83)90322-6. [PubMed: 6825952]

Kress C, Gautier-Courteille C, Osborne HB, Babinet C, Paillard L. Inactivation of CUG-BP1/CELF1 causes growth, viability, and spermatogenesis defects in mice. Mol Cell Biol. 2007; 27:1146–1157. http://dx.doi.org/10.1128/MCB.01009-06. [PubMed: 17130239]

Kumsta C, Hansen M. *C. elegans* rrf-1 mutations maintain RNAi efficiency in the soma in addition to the germline. PLoS One. 2012; 7:e35428. http://dx.doi.org/10.1371/journal.pone.0035428. [PubMed: 22574120]

L'Hernault, SW. Spermatogenesis; WormBook. 2006. p. 1-14.http://dx.doi.org/10.1895/wormbook.1.85.1

Lant B, Derry WB. Fluorescent visualization of germline apoptosis in living Caenorhabditis elegans. Cold Spring Harb Protoc. 2014; 2014:420–427. http://dx.doi.org/10.1101/pdb.prot080226. [PubMed: 24692492]

Lee MH, Schedl T. RNA-binding proteins. WormBook. 2006; 1:1–13. http://dx.doi.org/10.1895/wormbook.1.79.1.

Lettre G, Hengartner MO. Developmental apoptosis in C. elegans: a complex CEDnario. Nat Rev Mol Cell Biol. 2006; 7:97–108. http://dx.doi.org/10.1038/nrm1836. [PubMed: 16493416]

Li D, Bachinski LL, Roberts R. Genomic organization and isoform-specific tissue expression of human NAPOR (CUGBP2) as a candidate gene for familial arrhythmogenic right ventricular dysplasia. Genomics. 2001; 74:396–401. http://dx.doi.org/10.1006/geno.2001.6558. [PubMed: 11414768]

Li L, Zheng P, Dean J. Maternal control of early mouse development. Development. 2010; 137(6):859–870. http://dx.doi.org/10.1242/dev.039487. [PubMed: 20179092]

Lints, R., Hall, DH. Reproductive system, overview. WormAtlas. 2009a. ⟨http://dx.doi.org/10.3908/wormatlas.1.21⟩

Lints, R., Hall, DH. Reproductive system, somatic gonad. WormAtlas. 2009b. ⟨http://dx.doi.org/10.3908/wormatlas.1.22⟩

Loria PM, Duke A, Rand JB, Hobert O. Two neuronal, nuclear-localized RNA binding proteins involved in synaptic transmission. Curr Biol. 2003; 13:1317–1323. http://dx.doi.org/10.1016/S0960-9822(03)00532-3. [PubMed: 12906792]

Maris, C., Dominguez, C., Allain, FHT. The RNA recognition motif, a plastic RNA-binding platform to regulate post-transcriptional gene expression. FEBS J. 2005. http://dx.doi.org/10.1111/j.1742-4658.2005.04653.x

McGovern M, Yu L, Kosinski M, Greenstein D, Savage-Dunn C. A role for sperm in regulation of egg-laying in the nematode C. elegans. BMC Dev Biol. 2007; 7:41. http://dx.doi.org/10.1186/1471-213X-7-41. [PubMed: 17472754]

Merritt C, Rasoloson D, Ko D, Seydoux G. 3′ UTRs are the primary regulators of gene expression in the *C. elegans* germline. Curr Biol. 2008; 18:1476–1482. http://dx.doi.org/10.1016/j.cub.2008.08.013. [PubMed: 18818082]

Merritt, C., Seydoux, G. Transgenic solutions for the germline; WormBook. 2010. p. 1-21.http://dx.doi.org/10.1895/wormbook.1.148.1

Mignone F, Gissi C, Liuni S, Pesole G. Untranslated regions of mRNAs. Genome Biol. 2002; 3 (reviews0004.1-reviews0004.10).

Milne CA, Hodgkin J. ETR-1, a homologue of a protein linked to myotonic dystrophy, is essential for muscle development in Caenorhabditis elegans. Curr Biol. 1999; 9:1243–1246. [PubMed: 10556089]

Neidt EM, Scott BJ, Kovar DR. Formin differentially utilizes profilin isoforms to rapidly assemble actin filaments. J Biol Chem. 2009; 284:673–684. http://dx.doi.org/10.1074/jbc.M804201200. [PubMed: 18978356]

Papadopoulos JS, Agarwala R. COBALT: constraint-based alignment tool for multiple protein sequences. Bioinformatics. 2007; 23:1073–1079. http://dx.doi.org/10.1093/bioinformatics/btm076. [PubMed: 17332019]

Richter JD, Lasko P. Translational control in oocyte development. Cold Spring Harb Perspect Biol. 2011; 3:a002758. http://dx.doi.org/10.1101/cshperspect.a002758. [PubMed: 21690213]

Robertson SM, Lin R. The Oocyte-to-Embryo Transition. Germ Cell Development in C elegans. 2013:351–372.

Rose KL, Winfrey VP, Hoffman LH, Hall DH, Furuta T, Greenstein D. The POU gene ceh-18 promotes gonadal sheath cell differentiation and function required for meiotic maturation and ovulation in Caenorhabditis elegans. Dev Biol. 1997; 192:59–77. http://dx.doi.org/10.1006/dbio.1997.8728. [PubMed: 9405097]

Rual JF, Ceron J, Koreth J, Hao T, Nicot AS, Hirozane-Kishikawa T, Vandenhaute J, Orkin SH, Hill DE, van den Heuvel S, Vidal M. Toward improving Caenorhabditis elegans phenome mapping with an ORFeome-based RNAi library. Genome Res. 2004; 14:2162–2168. http://dx.doi.org/10.1101/gr.2505604. [PubMed: 15489339]

Savill J, Fadok V. Corpse clearance defines the meaning of cell death. Nature. 2000; 407:784–788. http://dx.doi.org/10.1038/35037722. [PubMed: 11048729]

Schumacher B, Hanazawa M, Lee MH, Nayak S, Volkmann K, Hofmann R, Hengartner M, Schedl T, Gartner A. Translational repression of *C. elegans* p53 by GLD-1 regulates DNA damage-induced apoptosis. Cell. 2005; 120:357–368. http://dx.doi.org/10.1016/j.cell.2004.12.009. [PubMed: 15707894]

Schupbach T, Wieschaus E. Female sterile mutations on the second chromosome of Drosophila melanogaster. II Mutations blocking oogenesis or altering egg morphology. Genetics. 1991; 129:1119–1136. [PubMed: 1783295]

Tijsterman M, Okihara KL, Thijssen K, Plasterk RHa. PPW-1, a PAZ/PIWI protein required for efficient germline RNAi, is defective in a natural isolate of C. elegans. Curr Biol. 2002; 12:1535–1540. [PubMed: 12225671]

Timchenko LT, Miller JW, Timchenko NA, Devore DR, Datar KV, Lin L, Roberts R, Thomas Caskey C, Swanson MS. Identification of a (CUG)(n) triplet repeat RNA-binding protein and its expression in myotonic dystrophy. Nucleic Acids Res. 1996; 24:4407–4414. http://dx.doi.org/10.1093/nar/24.22.4407. [PubMed: 8948631]

Timmons L, Fire A. Specific interference by ingested dsRNA. Nature. 1998; 395:854. http://dx.doi.org/10.1038/27579. [PubMed: 9804418]

Tsuda K, Kuwasako K, Takahashi M, Someya T, Inoue M, Terada T, Kobayashi N, Shirouzu M, Kigawa T, Tanaka A, Sugano S, Güntert P, Muto Y, Yokoyama S. Structural basis for the sequence-specific RNA-recognition mechanism of human CUG-BP1 RRM3. Nucleic Acids Res. 2009; 37:5151–5166. http://dx.doi.org/10.1093/nar/gkp546. [PubMed: 19553194]

Wolke U, Jezuit EA, Priess JR. Actin-dependent cytoplasmic streaming in C. elegans oogenesis. Development. 2007; 134:2227–2236. http://dx.doi.org/10.1242/dev.004952. [PubMed: 17507392]

WormBase: etr-1 [WWW Document]. URL ⟨http://www.wormbase.org/db/get?Name=WBGene00001340;class=Gene⟩ (accessed 1.1.17)

WormBase: unc-75 [WWW Document]. URL ⟨http://www.wormbase.org/db/get?Name=WBGene00006807;class=Gene⟩ (accessed 1.1.17)

Yigit E, Batista PJ, Bei Y, Pang KM, Chen CC, Tolia NH, Joshua-Tor L, Mitani S, Simard MJ, Mello CC. Analysis of the C. elegans Argonaute family reveals that distinct Argonautes act sequentially during RNAi. Cell. 2006; 127:747–757. DOI: 10.1016/j.cell.2006.09.033 [PubMed: 17110334]

Yu X, Lu N, Zhou Z. Phagocytic receptor CED-1 initiates a signaling pathway for degrading engulfed apoptotic cells. PLoS Biol. 2008; 6:0581–0600. http://dx.doi.org/10.1371/journal.pbio.0060061.

Yuan J, Shaham S, Ledoux S, Ellis HM, Horvitz HR. The C. elegans cell death gene ced-3 encodes a protein similar to mammalian interleukin-1β-converting enzyme. Cell. 1993; 75:641–652. http://dx.doi.org/10.1016/0092-8674(93)90485-9. [PubMed: 8242740]

Zhou Z, Hartwieg E, Horvitz HR. CED-1 is a transmembrane receptor that mediates cell corpse engulfment in C. elegans. Cell. 2001; 104:43–56. http://dx.doi.org/10.1016/S0092-8674(01)00190-8. [PubMed: 11163239]

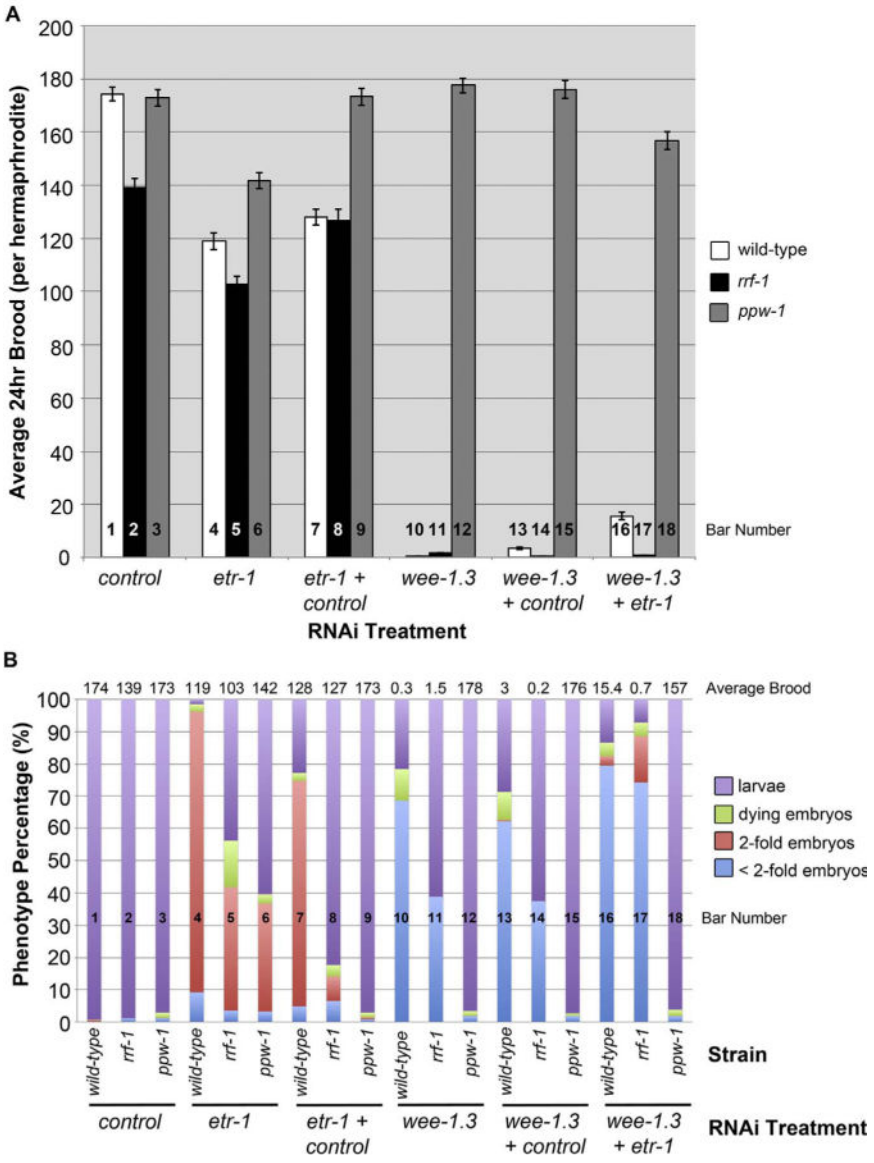


**Fig. 1.**

Depletion of ETR-1 results in a reduced brood that is dependent on a reduction in both the soma and germ line. Wild-type, *rrf-1(pk1417)* somatic RNAi defective mutants, and *ppw-1(pk1425)* germline RNAi defective mutants were fed bacteria expressing the indicated dsRNA to control, *etr-1*, *etr-1* and *control*, *wee-1.3*, *wee-1.3* and *control*, or *etr-1* and *wee-1.3* genes. (A) Average 24 h brood size per individual hermaphrodite for wild-type animals (white bars) compared to *rrf-1(pk1417)* mutants (black bars) and *ppw-1(pk1425)* mutants (grey bars) treated with the indicated RNAi constructs. For each RNAi treatment, brood data was collected from between 94 and 152 hermaphrodites. Each bar represents the average brood from at least 4 independent experiments and the error bars represent SEM. Statistics were determined using a Student's *T*-test and all p-values are provided in Supplementary Table S1. (B) Phenotypic characterization of the resulting broods of wild-type, *rrf-1(pk1417)* mutants or *ppw-1(pk1425)* mutants treated with the indicated RNAi

constructs. The average brood for each tested condition varies (see Fig. 1A) and is noted above the graph for easy recollection. Purple = larvae. Green = dying embryos. Red = 2-fold embryos. Blue = embryos younger than 2-fold stage.

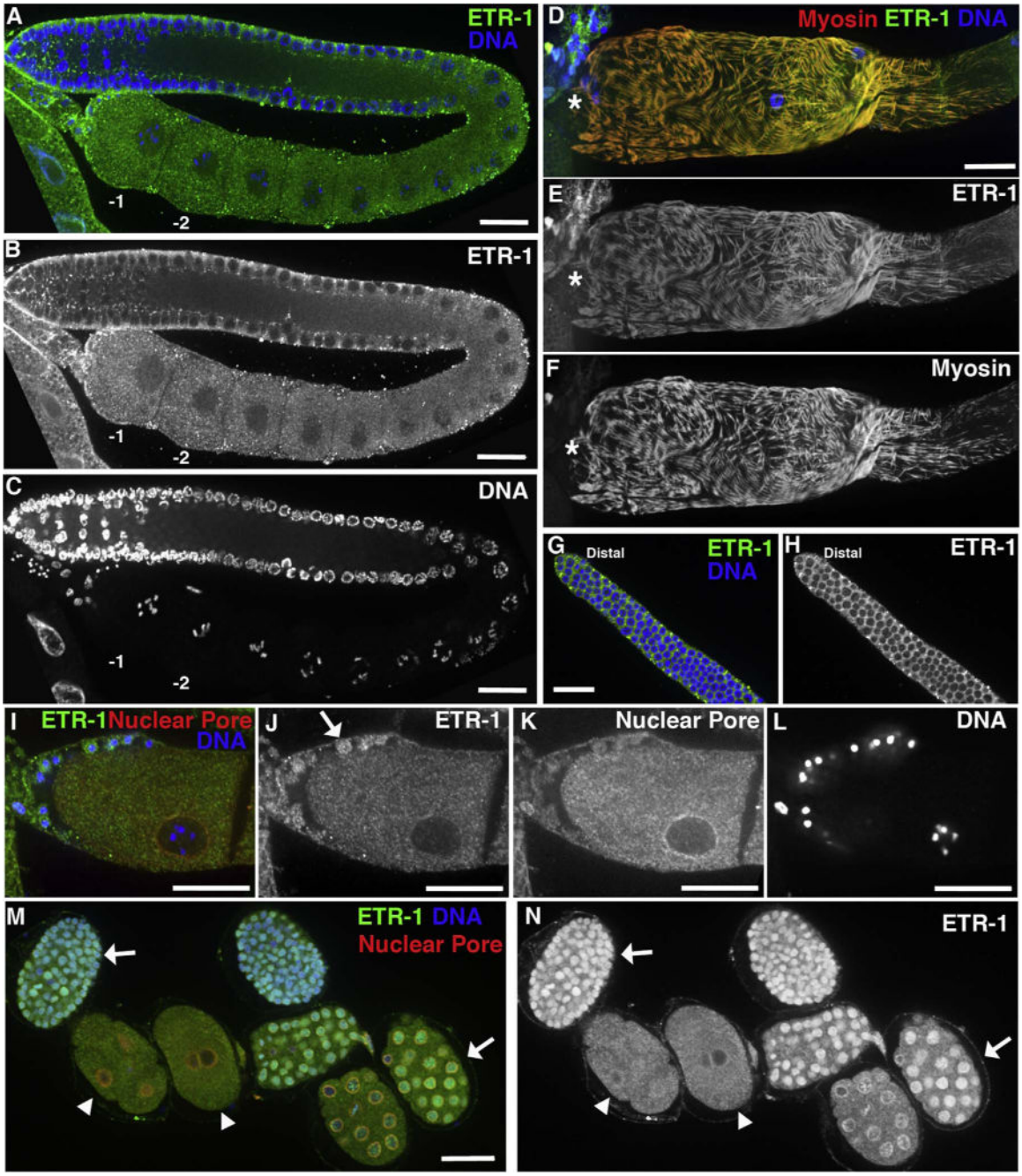


**Fig. 2.**

ETR-1 is expressed in the somatic gonad, germ line, and embryos. Confocal images of dissected wild-type gonads or embryos, fixed, and stained with the indicated antibodies. (A–C) Medial z-stack projection of gonad co-stained for ETR-1 (green in A) and DAPI for DNA (blue in A). Individual images of ETR-1 shown in (B) and DNA in (C). Positions of oocytes are indicated by −1 and −2. (D–F) Superficial z-stack projection of proximal gonad co-stained with ETR-1 (green in D), anti-MHCA for myosin (red in D), and DAPI for DNA (blue in D). Individual images of ETR-1 shown in (E) and myosin in (F). Asterisks indicates proximal gonad. (G–H) Superficial z-stack projection of distal gonad co-stained with ETR-1

(green in G) and DAPI for DNA (blue in G). Individual ETR-1 image shown in (H). (I–L) Single-plane medial image of the −1 oocyte and sperm co-stained for ETR-1 (green in I), nuclear pore (red in I), and DAPI for DNA (blue in I). Individual images of ETR-1 shown in (J), nuclear pore in (K), and DNA in (L). Arrow in (J) indicates sperm. (M–N) Z-stack projections of dissected embryos co-stained for ETR-1 (green in M), nuclear pore (red in M), and DAPI for DNA (blue in M). Individual ETR-1 image shown in (N). Arrowheads indicate early embryos (1- to 16-cell stage). Arrows indicate older embryos (> 32-cell stage). Scale bars are 20 μm.

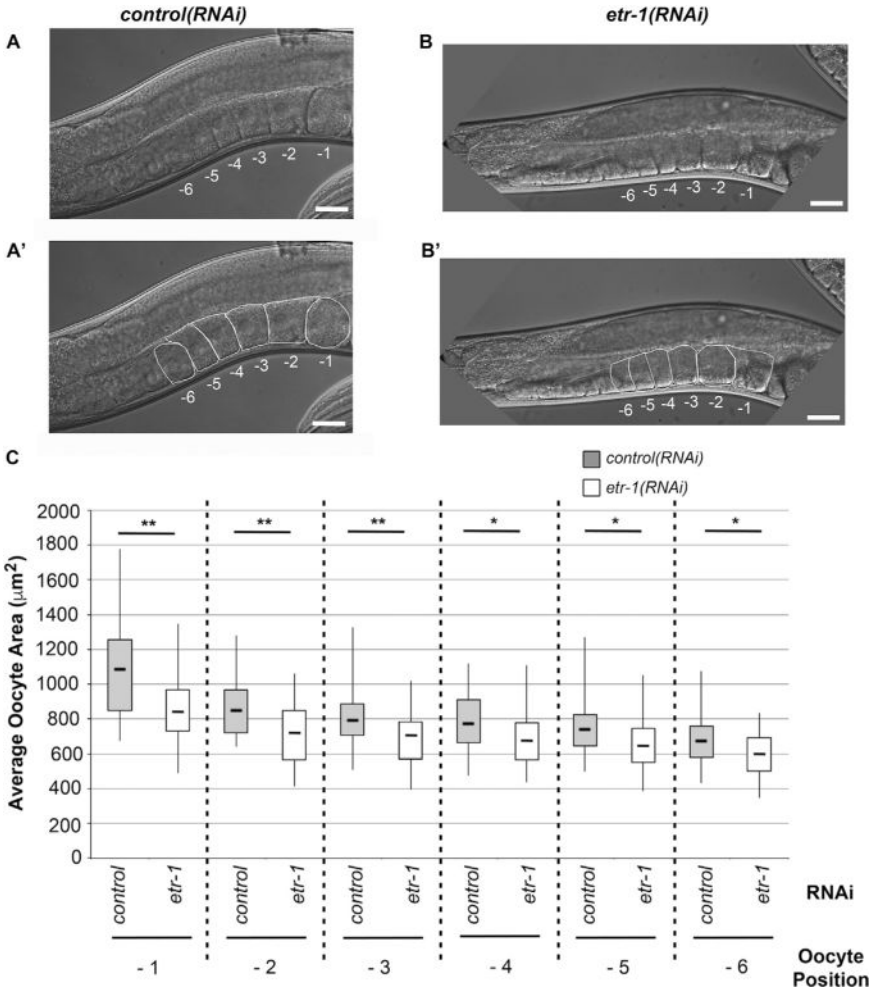


**Fig. 3.**

ETR-1 depletion results in a decrease in oocyte size. (A–B) DIC images of proximal gonads of wild-type animals subjected to either *control(RNAi)* or *etr-1(RNAi)*. The oocytes are labeled according to their position relative to the spermatheca, with the −1 oocyte being that closest to the spermatheca. In A′ and B′ we have outlined the area utilized in the representative examples to show how oocyte area was calculated. (C) Box-plot diagram showing the average oocyte area per position relative to the spermatheca in wild-type animals treated with either *control(RNAi)* (grey boxes) or *etr-1(RNAi)* (white boxes). The box represents the lower (Q1) and upper (Q3) quartiles, while the whiskers represent the minimum and maximum values. Medians are represented by the dark line within each box. Each bar represents the average of 3 independent experiments (n = 27–33 animals total) and statistics were determined using a Student's *T*-test. Double asterisks (**) denotes p-values < 0.005 and single asterisks (*) denotes p-values < 0.05 comparing control-depleted to ETR-1-depleted oocytes at each individual position.

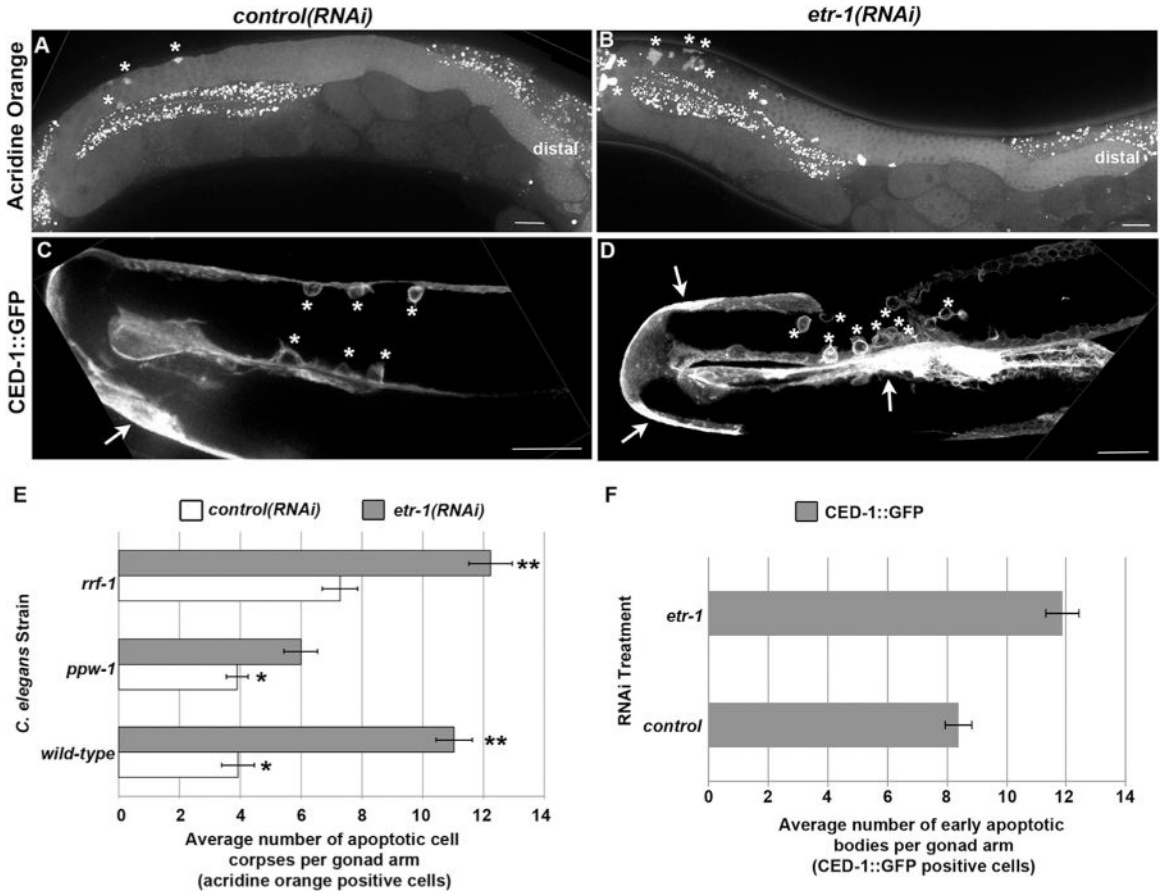


**Fig. 4.**

ETR-1 depletion results in increased apoptotic cells in the germ line. (A–B) Gonads of wild-type animals subjected to either *control(RNAi)* (A) or *etr-1(RNAi)* (B) were stained with acridine orange (white). Asterisks indicate apoptotic cells. The distal end of the gonad is indicated with the label “distal”. Staining outside the germ line in both conditions is background auto-fluorescence in the gut. (C–D) Live imaging of gonads of CED-1::GFP animals subjected to either *control(RNAi)* (C) or *etr-1(RNAi)* (D). Asterisks indicate early apoptotic cells. Arrows indicate gonadal sheath expression. Scale bars are 20 μm in all images. (E) The average number of apoptotic cell corpses as determined by acridine orange in wild-type, *ppw-1(pk1425)* mutants, or *rrf-1(pk1417)* mutants treated with either *control(RNAi)* (white bars) or *etr-1(RNAi)* (grey bars). (F) The average number of early apoptotic bodies as determined by CED-1::GFP positive expression in *control(RNAi)* and *etr-(RNAi)* gonad arms. For Panels E and F, the error bars indicate SEM; n-values are between 42 and 59 animals for each condition; statistics were determined using a Student’s *T*-test; and all p-values were < 0.001 unless denoted by asterisks which indicates compared values were not significantly different (* = p-value of 0.97, and ** = p-value of 0.19).

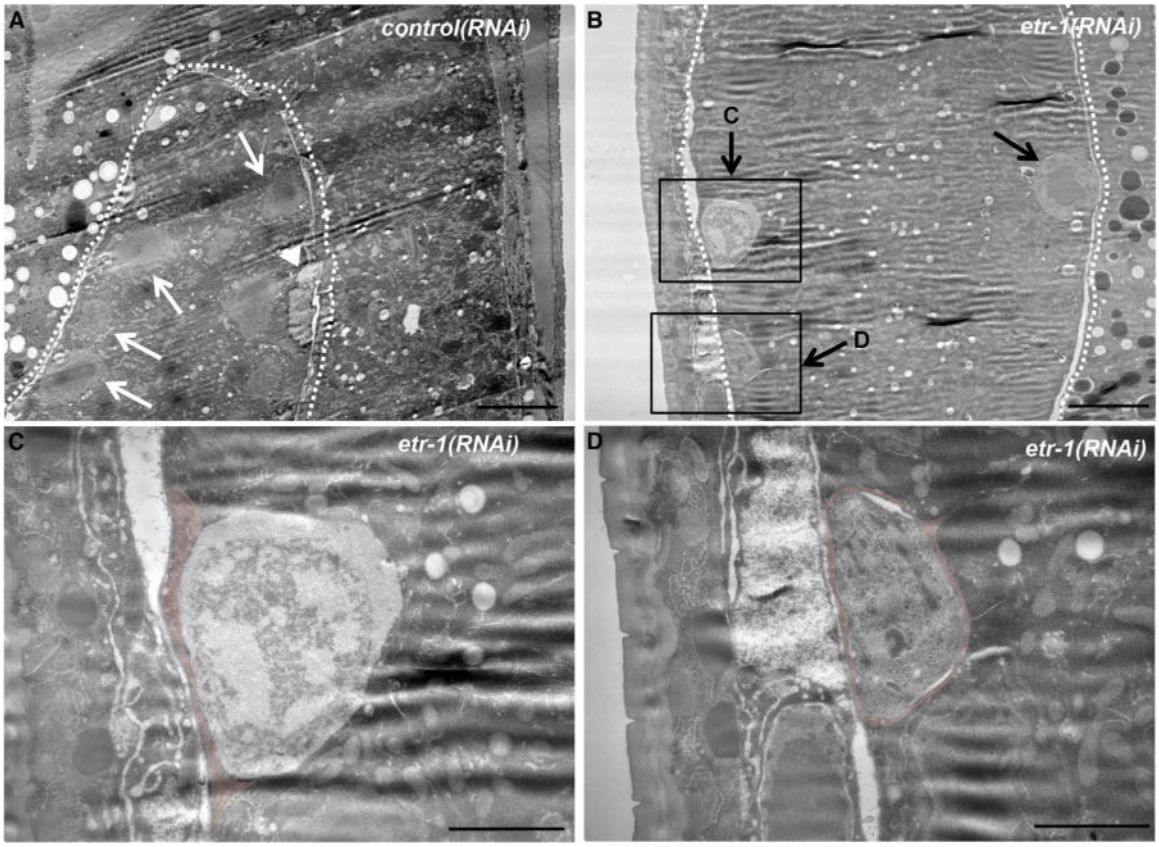


**Fig. 5.**

ETR-1-depleted animals exhibit incomplete engulfment of germline apoptotic cells. Transmission electron micrographs of germ lines from *control(RNAi)* (A) or *etr-1(RNAi)* animals (B–D). (A–B) Low magnification images of longitudinal sections of intact adult hermaphrodite gonads subjected to the indicated RNAi treatment. (A) TEM image through the gonad loop. The ventral portion of the loop is seen within the dashed line, with the unsheathed portion of the distal gonad arm lying to the bottom of the image, off-screen. White arrows point to healthy germ cells. White arrowhead points to gonadal sheath cell nuclei #2. (B) TEM image is to the gonad region immediately distal to the loop. Black arrows point to apoptotic germ cells. The regions boxed in panel B are magnified in C and D. (C–D) High magnification of apoptotic cells from *etr-1(RNAi)* animals. The sheath cell is pseudocolored in pink and fails to engulf the apoptotic cell in C but completely engulfs the apoptotic cell in D. Scale bars in A and B are 5 μm. Scale bars in C and D are 2 μm.

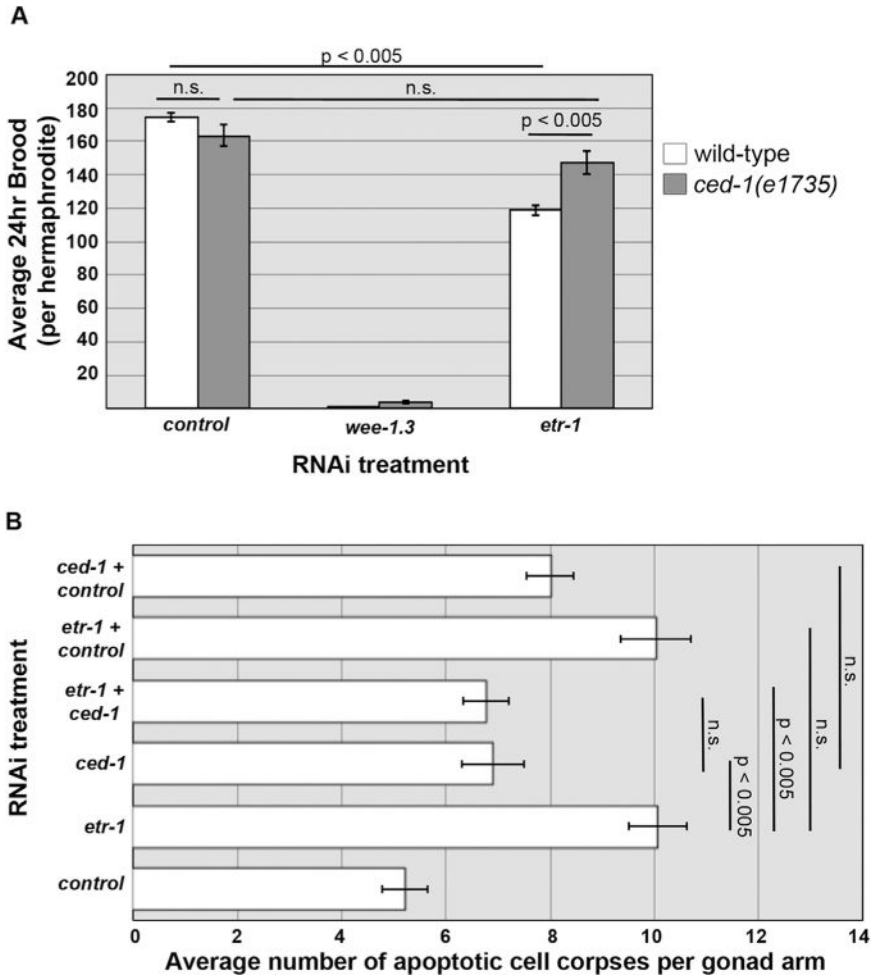


**Fig. 6.**

Co-depletion of CED-1 and ETR-1 suppresses the ETR-1 depletion phenotypes. (A) The average 24 h brood of wild-type (white bars) and *ced-1(e1735)* mutants (grey bars) treated with RNAi directed against: control, *wee-1.3*, or *etr-1* genes. (B) The average number of apoptotic cell corpses as determined by acridine orange staining of wild-type animals treated with RNAi directed against: *control*, *etr-1*, *ced-1*, *etr-1* and *ced-1*, *etr-1* and *control*, or *ced-1* and *control* genes. Each bar represents the average of 3 independent experiments (n = 20–47 gonad arms) and the error bars indicate SEM. Statistics were determined using a Student's *T*-test and p-values indicated.

## Table 1

ETR-1-depleted worms exhibit normal mitotic indices, ovulation rates, and gonad size.

| | ***control (RNAi)*** | ***etr-1 (RNAi)*** | **p-value** |
|---|---|---|---|
| Mitotic Index | 5.46 ± 0.31 | 4.86 ± 0.35 | 0.21 |
| Ovulation Rate | 3.98 ± 0.32 | 4.04 ± 0.24 | 0.88 |
| Uterus Length (μm) | 387.6 ± 10.6 | 367.3 ± 16.1 | 0.31 |
| Distal Gonad Length (μm) | 354.6 ± 20.2 | 313.3 ± 26.7 | 0.23 |

Mitotic index and ovulation rate were calculated as described in the Materials and Methods section. Uterus length is defined as the length of the uterus from one end to the other end. Distal gonad length is defined as the length from the distal tip cell (DTC) to the gonad bend. The number of animals analyzed were: n = 44–46 (mitotic index), n = 41–44 (ovulation rate), n = 41–49 (uterus length), and n = 40–42 (distal gonad length). Each value represents the average of at least 4 independent experiments and p-values were determined using a Student's *T*-test. Standard error of the mean (SEM) is reported.